Compression After Impact on Honeycomb Core Sandwich Panels with Thin Facesheets, Part 2: Analysis

Thomas D. McQuigg[1] and Rakesh K. Kapania[2]
Virginia Polytechnic Institute and State University, Blacksburg, VA, 24060

Stephen J. Scotti[3] and Sandra P. Walker[4]
NASA Langley Research Center, Hampton, VA, 23681

A two part research study has been completed on the topic of compression after impact (CAI) of thin facesheet honeycomb core sandwich panels. The research has focused on both experiments and analysis in an effort to establish and validate a new understanding of the damage tolerance of these materials. Part 2, the subject of the current paper, is focused on the analysis, which corresponds to the CAI testings described in Part 1. Of interest, are sandwich panels, with aerospace applications, which consist of very thin, woven S2-fiberglass (with MTM45-1 epoxy) facesheets adhered to a Nomex honeycomb core. Two sets of materials, which were identical with the exception of the density of the honeycomb core, were tested in Part 1. The results highlighted the need for analysis methods which taken into account multiple failure modes. A finite element model (FEM) is developed here, in Part 2. A commercial implementation of the Multicontinuum Failure Theory (MCT) for progressive failure analysis (PFA) in composite laminates, Helius:MCT, is included in this model. The inclusion of PFA in the present model provided a new, unique ability to account for multiple failure modes. In addition, significant impact damage detail is included in

---

[1] Graduate Research Assistant, Aerospace and Ocean Engineering, 215 Randolph Hall, Student Member AIAA
[2] Mitchell Professor, Aerospace and Ocean Engineering, 215 Randolph Hall, Associate Fellow AIAA
[3] Structures and Materials Cheif Engineer, Research Directorate, Mail Stop 162, Member AIAA
[4] Supervisory Research Aerospace Engineer, Structural Mechanics and Concepts Branch, Mail Stop 190, Member AIAA

the model. A sensitivity study, used to assess the effect of each damage parameter on overall analysis results, is included in an appendix. Analysis results are compared to the experimental results for each of the 32 CAI sandwich panel specimens tested to failure. The failure of each specimen is predicted using the high-fidelity, physics-based analysis model developed here, and the results highlight key improvements in the understanding of honeycomb core sandwich panel CAI failure. Finally, a parametric study highlights the strength benefits compared to mass penalty for various core densities.

Nomenclature

E = extensional Young's modulus

I = stress invariant

G = shear modulus

W = waviness coefficient

$[C]$ = constitutive matrix

ϕ_f = fiber volume fraction

ϕ_m = matrix volume fraction

σ = stress

ϵ = strain

υ = Poisson's ratio

a = equation coefficient

d = dent diameter

h_{max} = maximum dent depth

i = subscript indicator

x = global coordinate or axis, coupon width direction

y = global coordinate or axis, coupon load direction

z = global coordinate or axis, coupon through the thickness direction

I. Introduction

Lightweight structures, featuring composite sandwich materials, are increasingly being featured in the design of tomorrow's aerospace vehicles. Examples can be found in many types of aerospace vehicles, from small private propeller driven planes, to the newest commercial jetliners, to the next generation of heavy lift vehicles for future space exploration. Some of the major design challenges in composites pertain to damage repair, and ultimately, the understanding of damage formation and response of a composite structure with damage present. It is important, in this respect, to ascertain the damage tolerance of these sandwich structures. The current, two part research is focused on the understanding of the response of these materials to compression after impact (CAI).

In a related report [1], the first of these two parts was discussed, which focused on the experimental portion of this work. Two Nomex honeycomb core sandwich panel materials with thin woven fiberglass facesheets were introduced. These two materials were identical, except for the density of the Nomex honeycomb used in the core. The density of the honeycomb core, 3 lb/ft^3 in one material (3PCF-XX), and 6 lb/ft^3 in the other (6PCF-XX), was used to assess the core density's effect on damage formation and CAI response. Damage formation was studied using static indentation, and an impact survey using a drop tower. This information was used to select the energy levels of interest for impacts on CAI test coupons. Twenty four CAI test coupons were then subjected to end loaded compressive conditions until CAI failure occured. Two distinct failure modes were observed, indentation propagation and crack propagation, and the core density was shown to control the resulting failure mode.

In the current paper, the second of this two part research iniative is presented, which deals with a finite element model (FEM), developed for analyzing damage progression in sandwich structures. Due to the results of Part 1, it was concluded that a model with multiple failure mechanisms would need to be developed which could account for both failure modes seen previously. Before the new model was developed, the CAI models existing in the literature were considered. This review is briefly explained in the next section, and further information can be found in the Ph.D. Dissertation by McQuigg [2].

A. Current CAI Models

Currently available CAI models for thin facesheet honeycomb core sandwich panels include both analytic solutions and finite element models. Some of these solutions are very detailed, complex and time consuming. Also, the models focus on a single failure mode, mostly indentation propagation, and little effort has been expended to analytically study the competition between failure mechanisms in sandwich panels. Rather, attention is paid to experimental methods for picking the failure mode to model, and then analytically studying limited specific cases. The methods proposed in the current work will seek to expand upon this by including multiple failure modes within a single model.

Many of these models reference the analytic solution which was used by Minguet [3] to predict dimple propagation failure mode in thin-facesheet sandwich construction, by considering the effect of the residual dent and associated core damage on CAI strength. A continuum core model was implemented. Only the out of plane movement of the damaged facesheet, modeled by Classical Laminate Theory (CLT), was considered, while the undamaged facesheet's response was fixed in the out-of-plane direction. Core damage and propagation was represented as an assumed idealized version of a flatwise compression test response of a honeycomb core; this technique would be carried over into subsequent models. The resulting model over-predicted the CAI strength of the limited experimental data point presented in the paper. Minguet's model has proved to be complex in implementation and computationally intensive. The fidelity of subsequent analytic models has been reduced for computational efficiency, while still retaining many of Minguet's core ideas.

Tsang [4] offered a revision to the Minguet continuum core model that included an elastic foundation core. The Tsang model was described by two parameters used as a fit for the displacement and stress distribution in the through-the-thickness direction. A detailed experimental impact damage and CAI study of thin facesheet composite sandwich panel was presented. The resulting dimple propagation failure mode was simulated using the sandwich model with the two parameter core. It was found that the lack of accounting for facesheet damage and failure propagation contributed to an under-prediction of growth of the initial indentation and over-prediction of the final CAI strength. Xie and Vizzini [5] [6] offered a further revised version of the Minguet model with a simple one-parameter representation of the non-linear core crushing response. The out of plane stress

acting on the core is simply monitored until the core crush strength is exceeded. Once this occurs, the reaction force of the core is set to zero. It was shown that his model successfully captures the correct propagation of core damage. The authors concluded that the level of safety of a composite structure could be expressed mathematically with respect to a critical far field stress based on an experimental calibration at a known sensor location. The authors also assumed that the significance of facesheet damage was negligible to the dimple propagation failure mechanism in thin facesheet sandwich panels and did not include initial or progressive facesheet failure.

Other researchers have turned to finite element modeling (FEM) as a means of including more realistic damage, while still limiting implementation complexity and computational time. Ratcliffe and Jackson [7] have expanded on the work and input of Minguet, Tsang, Xie *et al.* through a simple FEM which includes a shell element represented face-sheet and a non-linear spring element model for the elastic support provided by the core. Impact damage in this model was modeled as a geometric dent included in the facesheet and a region of damaged core elements based on the idealized core crush response of damaged honeycomb core. However, during their work they found that the included "damaged" spring element core region resulted in a gradual global failure which was dissimilar to the case study experimental results they presented as well.

Hwang and Lacy [8] also considered the analytic work of Minguet and others and created a FEM approach for predicting the CAI strength of similar honeycomb core panels. Non-destructive techniques were used to estimate material property degradation due to the initial impact damage and honeycomb core crush tests were used to obtain a non-linear transverse core behavior for implementation. The expected CAI strengths were consistently under-predicted by the model for these panels. The authors also briefly considered facesheet failure during CAI strength prediction with their FEM model using a maximum stress criterion for individual elements. This was effective for predicting the onset of facesheet failure, but was not able to model progressive facesheet failure. An earlier attempt at FEA was done by Shyprykevich, Tomblin, Raju *et al.* [9]. Two models were developed, one in ABAQUS, and one in ANSYS. Both models used solid continuum core models similar to others that have been developed. Also, both needed calibration with experimental data in order to obtain their accuracy. Facesheet failure was briefly considered, but not fully developed.

Xie and Vizzini also considered FEA techniques. In one reference [10], they focus on local strain results and comparison to experiment in order to make residual strength redictions. In an earlier attempt [11], the authors had focused on delamination as a failure mode, which is not a topic in the current research.

On the more detailed end of the analysis spectrum, one further model should be mentioned as an example. By making use of the implementation efficiency of modern computers, Czabaj, Zehnder, Davidson *et al.* [12] presented an ultra-high fidelity FEM approach to CAI strength prediction. The complex model included geometrically accurate representations of a honeycomb core. The geometrically accurate region was located in the region of expected failure only, and the rest of the core was modeled with solid orthotropic elements to increase the computational efficiency of the model. In addition to predicting the CAI strength, the researchers also wished to correctly model the sandwich panel's response to quasi-static indentation and found that the accurate geometric depiction of the core provided an improved response to this loading condition over a smeared property solid isotropic core model. The transverse response of the core was modeled after an idealized flatwise core compression experimental result, as in other models mentioned. The resulting model provided an excellent match to experimental quasi-static indentation data from tests on the sandwich constructions they sought to model.

The methods used to model the honeycomb core in current CAI models often involves the simplication of its response to flatwise compression. In more complex cases, it also requires a homogenized, continuum representation of its linear elastic orthotropic response. A well known reference on the subject of cellular solids, such as hexagonal pore honeycomb structures, is the book by Gibson and Ashby [13]. The authors provide a method of calculating the effective homogenized material properties of honeycomb core based on the two dimensional bending response of cell walls. Some of this theory will be given later in this paper. The transverse non-linear response of hexagonal cell honeycomb core due to an out-of-plane crushing load has also been incorporated into various CAI strength prediction models in an idealized form. A good explanation of honeycomb core crushing behavior using experimental and numerical results was presented by Aktay *et al.* [14]. They showed the stages of core crush in Nomex and Aluminum honeycomb cores, including buckling initiation,

progressive folding, and finally, densification using experimental examples. Gornet, Marguet, and Marckmann [15]; Heimbs [16]; and Kaman, Solmax, and Turan [17] also developed computationally implemented models for honeycomb core crush response with good results. The current model will implement an idealization of the flatwise compression response showed experimentally in these works.

B. Progressive Failure Analysis

In the present research, an implementation of progressive damage modeling is included for damage modeling in the facesheets of the FEM. Although the analysis of composite laminate stress and strains is well understood, the analysis and prediction of fiber reinforced composite failure is less well understood. Many methods exist, but there is no universally accepted criterion. As explained by Dávila, Rose, and Iarve [18], this is due to the varied nature of discrete damage events in a fiber reinforced laminate and high degree of variability in laminate construction. The type of damage events which are pertinent to the present research were previously discussed in the sections concerning impact damage in composite laminates and sandwich panels. In addition to the degree of variation in the types of damage and orientation possible, the treatment of the analysis and prediction of the formation and propagation of this damage varies with scale of the idealization. A meso-scale model is used in the present research. Meso-scale models are popular for being both more computationally advantageous than micromechanics models, as well as more detailed and accurate than structural scale models.

A continuum damage mechanics (CDM) model is used in the current research, which was discussed by Dávila, Rose, and Iarve [18] with respect to its advantages and disadvantages. CDM generally assume homogenous, orthotropic plies and corresponding damage modes. When analysis predicts a damage event, a soft discontinuity is imposed in the form of a stiffness reduction to the damaged material. The failure criteria and material degradation used are often associated with a particular mode of failure. Other damage phenomenon, such as fiber-matrix disbond and fiber kinking are taken into account through techniques such as co-current analysis of a micromechanics model and *in situ* strengths, respectively. The authors argue that CDM suffers from over-propagation of

inter-fiber fracture (IFF), and mesh dependence.

Two important components, as described by Puck and Schürmann [19], of any laminate strength analysis are, that they are close to physical reality, and that they are simple enough for computationally efficient implementation in engineering design work. The authors also succinctly describe the requirements of a progressive failure analysis (PFA) which applies to the method of implementation in the current research. Stress and strains must first be analyzed ply by ply. In the present research this will be done through the use of classical laminate theory (CLT). A fracture criterion is applied to single plies. A degradation model must then be utilized which includes the effects of material fractures which may not lead to ultimate laminate failure. Finally, the previously mentioned requirements of the PFA must be implemented iteratively through the use of a computer program.

Puck and Schürmann [20] included in their work a heavy investigation of IFF mechanisms, with special focus on the orientation of matrix cracks and the consideration of stress with respect to the fracture plane. This work involved consideration of micro-mechanics. Attempts to account for the effects of micro-mechanics in CDM models led to the use of multi-continuum theories (MCT), such as the MCT developed by Garnich and Hansen [21]. MCT provides a simple way of calculating fiber and matrix average stress states based on the laminate average stress state. A failure criterion for composite laminates which makes use of MCT was later developed by Mayes and Hansen [22]. The main benefits of MCT are that composite contituent failures are predicted by constituent stresses, and a robust progressive failure analysis is done through the use of soft discontinuities. When constituent level failure occurs within a model, the model structure remains intact and the resulting redistribution of load in the model can easily be evaluated. In the current model, MCT failure theory is implemeneted through the use of the commercial software Helius:MCT [23], developed by Firehole Composites.

C. Overview of Part 2 of the Research

In the rest of this document, the development of the present CAI model is explained, which is Part 2 of the current research. In the next section the new model will be introduced. The implementation of the honeycomb core behavior and compressive failure will be developed. The

progressive failure analysis in the facesheets will then be described. In addition, detailed impact damage is incoporated into the model based on the previous experimental results.

Subsequently, in the following section, the analysis results, which were produced using the present CAI model, are discussed. Twenty four analyses were completed which correspond to the experimentally tested coupons and the experimental and analysis results are compared for FEM validation. Finally, analysis results are presented for a parametric study which provides insights on the effect of the honeycomb core density on panel response.

II. Development of the CAI Analysis Model

In the current finite element model (FEM) for the prediction of CAI failure in honeycomb core sandwich panel coupons has been developed in the current research. The major contributions of the new model include increased fidelity of impact damage physical attributes, and implementation of a progressive failure analysis for facesheet damage. Other components of the model are similar to previous models. The inclusion of both a facesheet and a core failure mechanism allows the model to predict the two failure modes seen in the experimental test results in Part 1 [1] of the current research. The introduction to the present model will begin with the geometry and boundary conditions.

A. Model Overview

A FEM was developed for analysis of the CAI response of honeycomb core sandwich panel coupons using the commercial FEA code ABAQUS/Standard. The FEM includes representations of both front (damaged) and rear facesheets, as well as a continuum solid representation of the homogenzied, honeycomb core. Only one quarter of the sandwich panel coupon was modeled due to the assumption of symmetry of the impact damage present in the front facesheet, and the expected failure modes. A global coordinate system was established in the following manner. If the two major dimensions (i.e. length and width) of the sandwich panel plate are located in the $x-y$ plane of a Cartesian coordinate system, where the loading direction is parallel to the y-axis, only the top right quarter of the sandwich panel coupon is modeled. This is the region located in the Cartesian quadrant where points are defined by positive x and positive y coordinates. The length of the model

in the y-direction is then $l/2$ where l is the length of the coupon modeled. Likewise, the width in the x-direction modeled is $w/2$, and the thickness is $(t_c + 2t_f)$ where w is the coupon width, t_c is the thickness of the core, and t_f is the facesheet thickness. The area of the model used to simulate impact damage will thus be located on the front facesheet on the z-axis of the global coordinate system, as highlighted in Fig. 1.

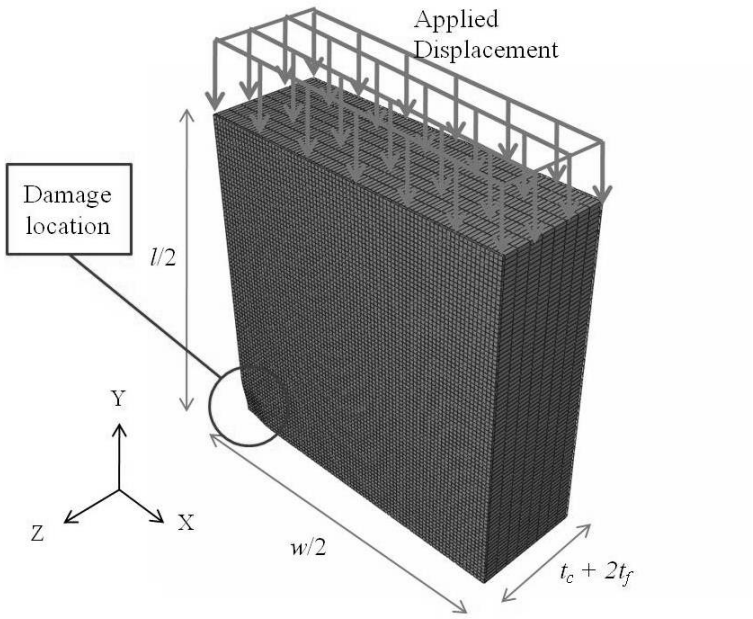

Fig. 1 New CAI model: FEM Geometry.

The following boundary conditions were used in the current model. It is required that the element node points located along the line $x = 0$ be fixed in the x-direction for symmetry in this direction. For y-direction symmetry, nodes along the line $y = 0$ are fixed from displacement in the y-direction. Rotational boundary conditions are not necessary for any node points, since the elements used are defined using only displacement degrees of freedom. A third initial boundary condition was applied at the facesheet nodes located at $(x, y = l/2, z)$, to simulate the effects of the coupon clamp and potting described in Part 1 of the research on experiments. Only at these locations on the facesheet, the nodes were restricted from displacement in the out-of-plane, z-direction. During the analysis step, loading was applied to the nodes located at the coordinates $(x, y = l/2, z)$ using an applied displacement boundary condition to simulate the displacement controlled loading used in CAI experiments. The nodal locations of the boundary conditions used in the new CAI model

are shown in Fig. 2 as enlarged nodes superimposed on the FEM.

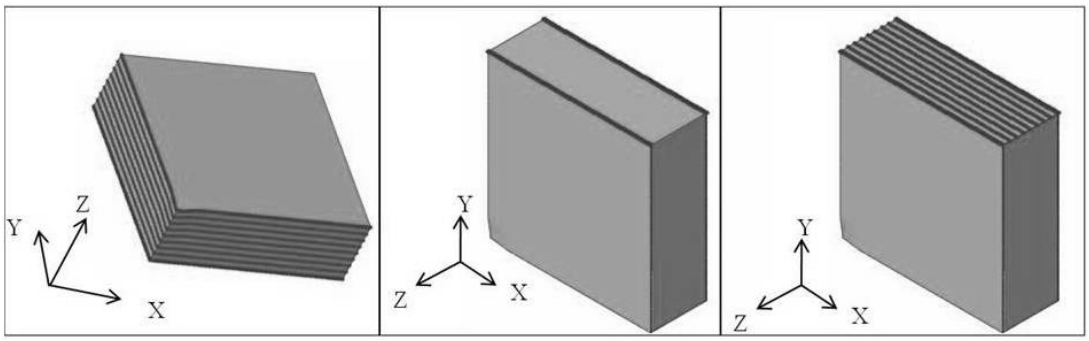

Fig. 2 New CAI model: FEM nodal locations for the boundary conditions for symmetry (left), simulated potting (center), and applied displacement (right) are shown as enlarged black dots on the solid sandwich panel geometry.

Shell elements and solid brick elements were used to model the facesheets and the core of the sandwich panel, respectively. The ABAQUS continuum shell element, *SC8R*, was used in the finite element representation of the sandwich panel facesheets. The main benefit of continuum shell elements over conventional shell elements is the explicit consideration of the shell thickness. In the continuum shell formulation, only displacement degrees of freedom are considered. The *SC8R* elements are a reduced element formulation that increases the computational efficiency, while making marginal accuracy sacrifices, if any, due to the location of the Gauss integration points. The constitutive response of the element shell section is defined as in classical laminate theory (CLT). Each ply layer of the composite shell section was defined using orthotropic engineering constants found from various experimentally derived material data available in the literature. The exact material constants are described later.

The 8-node, solid brick, ABAQUS finite element, *C3D8R*, was used to represent the honeycomb core of each sandwich panel CAI test coupon, which was modeled as a homogenized, continuum region. The elastic response of this element was implemented using nine orthotropic engineering properties to represent the constitutive model. The out-of-plane modulus, the L-direction shear modulus, and W-direction shear modulus for the corresponding honeycomb core are defined as experimentally determined constants. More details are given later. The in-plane extensional moduli and shear modulus for the continuum representation were determined using the theory described

by Gibson and Ashby [13]. Since, a non-linear model was necessary for the out-of-plane response of the homogenized core, an ABAQUS subroutine, UMAT, was written in FORTRAN to implement both the linear elastic response and the idealization of the non-linear flatwise core crush curve. The implementation of the core response by UMAT will be described in the next section.

B. Honeycomb Core Behavior

The linear elastic orthotropic response as well as the non-linear crushing failure of the core was implemented using the ABAQUS user subroutine, UMAT, which is written in the FORTRAN programming language. As written, the UMAT requires the following inputs to be read from the ABAQUS/Standard input file. First, the nine orthotropic engineering constants are given which define the linear elastic response of the material. The 10^{th} value is a constant which acts as a marker for the material point which defines it as either a "damaged" or "undamaged" material point. This is only with respect to the initial material model, and does not change with the results of any subsequent failure analysis. The flatwise core crush strength of the material, given as the associated failure strain value is the 11^{th} material constant. Finally, the 12^{th} material property sets the stress reduction in the element which results when an element is determined to have failed from out-of-plane compressive loading during an analysis step. This stress reduction is also defined by experimental data (i.e. a flatwise core crush test result for the stress-strain response).

Experimental flatwise core crush results for Nomex material generally show a brittle wall collapse and folding which results in a succession of rising and falling stress resultant for a displacement controlled test [14] [15] [16] [17]. This behavior is averaged to a single stress value, which was selected based on the idealization of core crush experimental results. Once the initial crush strength has been reached, successive cell wall collapse occurs at a much lower level of applied load since the cell wall stability has been compromised. Cell wall densification, and the corresponding eventual increase in crush stiffness, are not modeled in the present analysis, since the level of core deformation required is normally not reached in sandwich panel CAI response. For all current analyses, after failure, the stress tensor components are reduced to a predetermined percentage of their initial values. All extensional and shear moduli are set to zero so the stress remains constant after failure, resulting

in perfectly plastic response for any remaining deformation. The non-linear crush response in the z-direction for a 3 lb/ft^3 Nomex honeycomb was approximated by the idealized core crush response shown in Fig. 3. The 6 lb/ft^3 core response used is similar, except the appropriate constants are used for the higher linear elastic modulus and the higher core crush strength. The dashed and solid curves in Fig. 3 represent the response of impact damaged and initially undamaged core elements, respectively. A marker, which was previously mentioned as the 10^{th} subroutine input, determines which curve is used for a given material point.

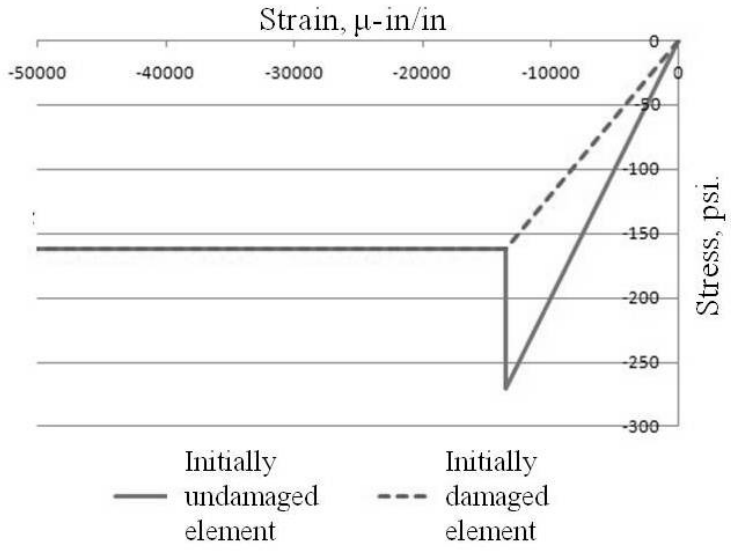

Fig. 3 Idealized core crush response use to define non-linear constitutive core behavior of 3 lb/ft^3 Nomex core.

C. Progressive Failure Analysis

Special consideration is given to the front, impact damaged facesheet in the form of the progressive failure analysis (PFA), accomplished through the Helius:MCT software [23]. This failure analysis allows the prediction of damage propagation during CAI failure, which simulates the appearance of a crack. The use of Helius:MCT does not change the element formulation or the constitutive model. It simply requires the explicit specification of various material and element properties, some of which are normally automatically calculated by the ABAQUS/Standard solver. The use of Helius:MCT requires a special material file written using the Firehole Composites auxiliary software,

"Helius Material Manager." The Material Manager determines the *in situ* properties of the lamina's fiber and matrix constituents based on the material constants provided, usually from experimentally determined sources for a given material. The *in situ* properties are calculated through MCT [21]. It is assumed that the average stress state, σ, of a representative volume element representative of the composite lamina can be expressed with respect to the matrix and fiber constituent average stress states, σ_m and σ_f, and the matrix and fiber volume fractions, ϕ_m and ϕ_f, as in Eq. 1.

$$\sigma = \phi_f \sigma_f + \phi_m \sigma_m \tag{1}$$

Using a "decomposition" of the laminate average stress state through MCT, the constituent average strain states can then be expressed as in Eqs. 2 and 3.

$$\{\epsilon_m\} = \frac{1}{\phi_m} \left([C_m] - [C_f]\right)^{-1} \left([C] - [C_f]\right) \{\epsilon\} \tag{2}$$

$$\{\epsilon_f\} = \frac{1}{\phi_f} \left(\{\epsilon\} - \phi_m \{\epsilon_m\}\right) \tag{3}$$

The constituent average stress states can then be found by the appropriate linearized constitutive relationships.

The above relationships are presented in the form of MCT used for unidirectional composite materials, but the MCT decomposition of woven fiber materials, like used in the present research, is essentially identical. Three sequential decompositions are required. Once these three decompositions are completed, the following average stress states are obtained for woven fiber composites [21]:

1. Fill tow matrix constituent average stress state
2. Fill tow fiber constituent average stress state
3. Warp tow matrix constituent average stress state
4. Warp tow fiber constituent average stress state
5. Matrix pockets constituent average stress state

Once the constitutent average stress states are obtained, they are used with experimentally determined lamina strengths to predict the onset of failure by the MCT failure theory developed by

Mayes and Hansen [22]. The MCT failure theory has a quadratic general form as in Eq. 4.

$$a_1 I_1^2 + a_2 I_2^2 + a_3 I_3 + a_4 I_4 = 1 \tag{4}$$

Here, a_i are coefficients related to the lamina strengths, and I_i are the transversely isotropic stress invariants described by Hashin [24]. These invariants are essentially a version of the classic stress invariants which are only valid for rotations of the stress tensor about the fiber oriented axis.

When failure is predicted for a constituent, the material properties for that constituent are instantly degraded. Matrix properties are reduced by 90% and fiber properties are reduced by 99%. The lamina properties for that material point are then recalculated using the degraded material properties for that constituent and the intact or degraded material properties for the other constituent materials. These new properties are then used by the ABAQUS/Standard solver to recalculate the stress state. In an iterative process, the new stress state is then resubmitted to Helius:MCT to update the material failure. This process is continued for an analysis step until convergence has been reached. The material states that are available to the solver are as follows, which can be found in the Helius Theory Manual [25]:

1. All constituents intact
2. Failed fill tow matrix constituent
3. Failed warp tow matrix constituent
4. Failed fill and warp tow matrix constituents
5. Failed fill tow fiber and matrix constituents
6. Failed warp tow fiber and matrix constituents
7. Failed fill tow fiber and matrix constituents, and failed warp tow matrix constituent
8. Failed warp tow fiber and matrix constituents, and failed fill tow matrix constituent
9. Failed warp and fill tow fiber and matrix constituents.

D. Impact Damage Modeling

The type and amount of impact damage present in a CAI specimen will determine its residual strength. The treatment of impact damage in the FEM is the subject of the present section. The most commonly included type of impact damage in CAI models is the residual dent resulting from a low velocity impact. In the present research, a residual dent is included in the FEM using measurements from the corresponding experimental test data for the dent's maximum depth and maximum diameter. Based on symmetry, only one quarter of the residual dent is modeled, and the dent is assumed to be circular. The indentation modeled affects the facesheet geometry, as well as the core geometry, and their resulting finite element meshes. The contour of the dent at the front facesheet to core interface is defined using Eq. 5 where the maximum dent depth, h_{max}, and dent diameter, d, are necessary inputs into the model, and x and y are the Cartesion coordinates. The through the thickness nodal locations of the continuum core are adjusted so equal spacing is maintained for element node locations between the indented top surface and the lower surface. A close up view of the geometry of the initial indentation included in the facesheet is shown in Fig. 4.

$$z = \frac{-h_{max}}{2}\left(1 + \cos\left(\frac{2\pi\sqrt{x^2+y^2}}{d}\right)\right) \tag{5}$$

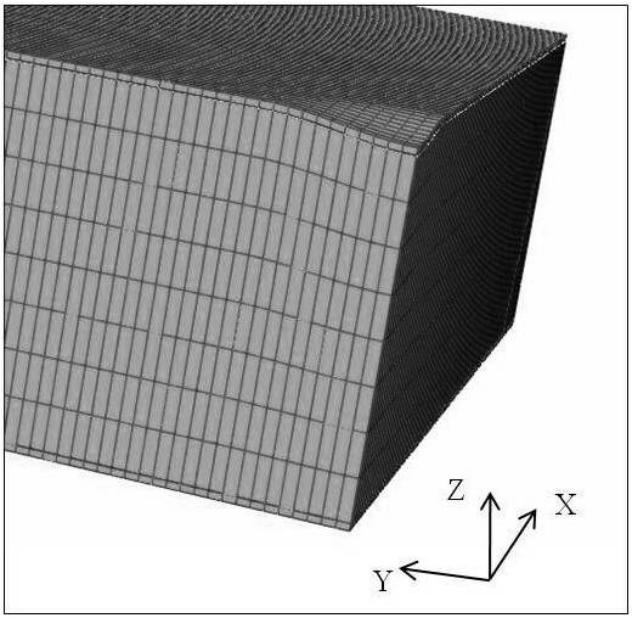

Fig. 4 Close-up view of indented region of FEM.

In the present research, additional damage details are included in the FEM. The impact damage

model described here attempts to simulate the presence of the various types of damage seen in the tested materials, discussed in Part 1 [1] of the research. Types of damage observed in the facesheets of the present materials of interest include delaminations, longitudinal matrix cracks, transverse fiber cracks and facesheet penetration. Types of damage observed in the core of the sandwich panels include brittle fracture of the cell walls, buckling of the cell walls, and voids in the cellular material where the cellular structure had been completely crushed. The effect of each of these damage types can be included in the model on a macroscopic level by degradation of the constitutive material properties of the corresponding damaged region (e.g. damaged facesheet region, or damaged core region). These regions must be defined by both their dimensions and the proper material property degradation amount. Both of these will now be described, first with respect to the damaged core region, and second, with respect to the damaged facesheet region.

Typical core damage from low velocity impact damage is shown in Fig. 5. The damaged core region is assumed to be circular in shape and concentrically located with respect to the residual dent previously discussed. It can therefore be described geometrically using a maximum radius and depth, measured from the front, damaged facesheet. The measurements used for this definition are taken from the low velocity impact damage survey corresponding to the specific material modeled. The impact damaged core region is assumed to be uniform in depth, to simplify the FEM input file definition. This assumption represents a conservative estimate of the size of the damaged core region.

An example of the damaged core region included in the new FEM model is shown in Fig. 6. In addition to the geometric definition of this region, the damage also requires a set value for the material property degradation (i.e. an element stiffness reduction). In the present research, it is assumed that the stiffness of the damaged core region is 60% of the initial properties. This was based on the idealization of stress-strain curves found by flatwise core crush test of similar materials used by Ratcliffe and Jackson [7]. The effect of the uncertainty of this value are discussed in the Appendix.

Images from microscopy of impact damaged test coupons in Fig. 7 shows the variation in facesheet damage between lightly damaged and more heavily damaged test coupons. In the more

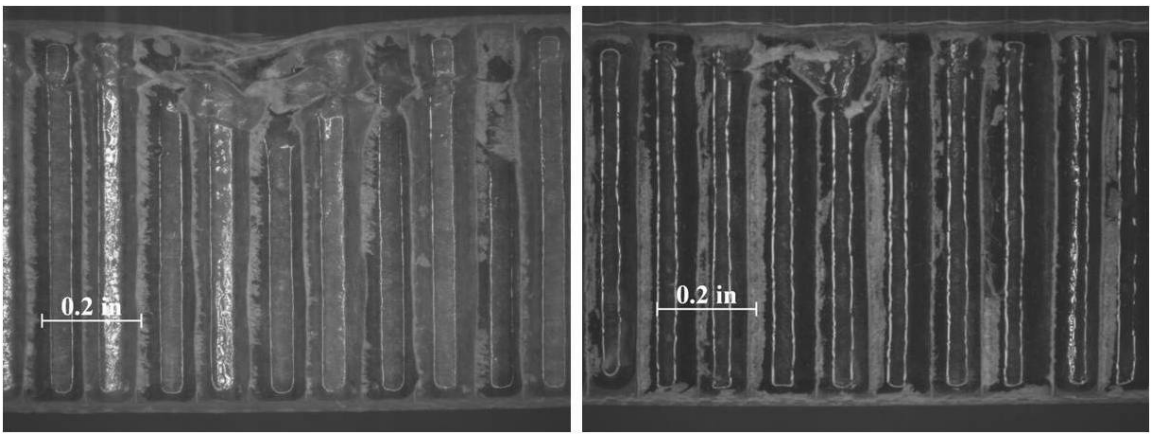

Fig. 5 Examples of core damage from optical microscopy of 3PCF-XX (left) and 6PCF-XX (right) series materials.

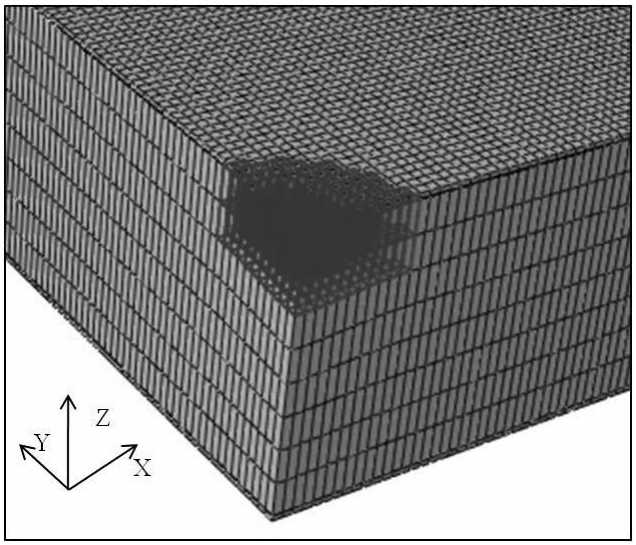

Fig. 6 Damaged core region in the FEM.

heavily damaged coupons, a region of facesheet fracture (failed fibers and matrix) is readily apparent. To incorporate these differences, the damaged facesheet region of the new model is actually two separately defined element groups. First, a region of moderate facesheet damage is included in all CAI test coupon models based on the location of inter-fiber fracture (IFF) or matrix cracking found from observations and measurement by optical microscopy. The area of matrix-damaged facesheet incorporated in the new FEM for CAI analysis is assumed circular and concentrically located with respect to the facesheet dimple. Geometrically, it is only necessary to define this region by an experimentally determined diameter. Matrix constituent material properties are degraded, which is

discussed later.

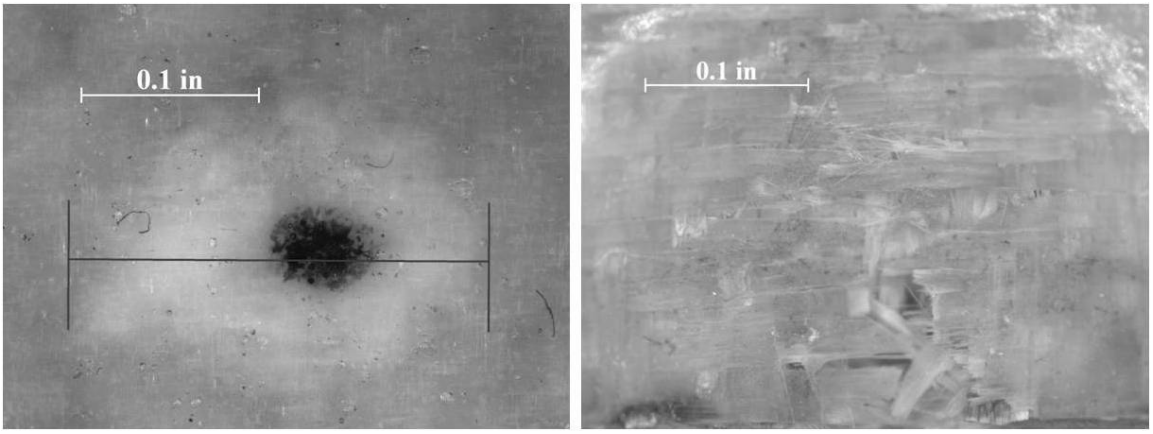

Fig. 7 Examples of light (left) and heavy (right) facesheet damage.

The second region of facesheet damage is only modeled for heavily damaged sandwich panels, where facesheet fiber fracture was observed. This region is assumed to be one element wide in the coupon load (y-)direction, and is defined in the coupon width (x-)direction by the corresponding length measured during experimental testing. In this region, both fiber and matrix constituent properties are degraded, which is discussed in more detail later. The geometric representations of the two damaged facesheet regions used in the new FEM model to represent impact damage prior to any compressive loading is shown in Fig. 8.

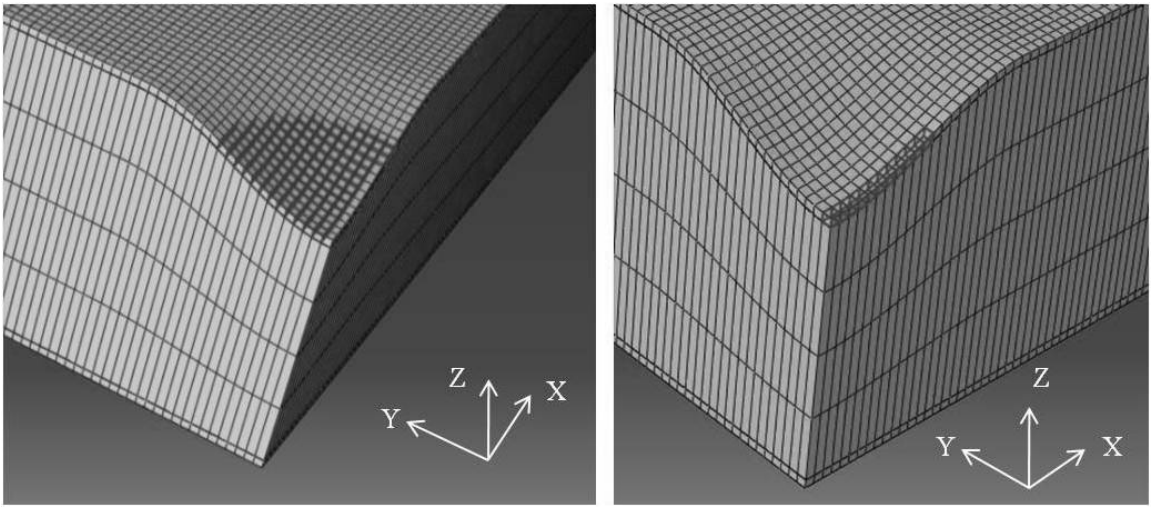

Fig. 8 FEM facesheet element regions representing areas of observed IFF (left) and fiber fracture (right).

The stiffness reductions in the two damaged facesheet regions of the FEM are calculated as follows, which is based on the values used by Helius:MCT for the PFA. In the matrix damaged region, the matrix constituent properties are reduced by 90% of their intial values. In the fiber fracture region, the matrix constituent properties are reduced by 90%, and the fiber constituent properties are reduced by 99%. The constituent material properties which are used are the *in situ* properties determined by the Helius Material Manager. Once the appropriate stiffness reduction has been applied to the fiber and matrix constituent material properties associated with each region, the damaged laminate level material properties are calculated as follows, which is unique to the impact damage modeling used in this research.

The following involves the calculation of effective moduli of woven composites, for which there are no widely accepted micromechanics relationships. The principal focus of establishing the appropriate relationships has centered on strategies to estimate the effects of waviness on woven lamina engineering properties. Some examples can be seen in the work by Whitcomb and Tang [26], Searles, Odegard, and Kumosa, [27], Gao, Li, and Mall [28] and Angioni, Meo, and Foreman [29]. Since this development is not the subject of the current research, a very simple method has been used in this research based on the micromechanics of unidirectional composites, classical laminate theory (CLT), and a correction or "waviness" factor.

A ply layer of epoxy matrix pre-impregnated woven fiberglass is considered as a four layer composite laminate. Four plies are considered instead of two so that the laminate can be considered balanced and symmetric. This allows for appropriate engineering constants to be easily calculated from CLT. The stacking sequence of unidirectional layers used to represent a single woven layer is $[0/90]_S$. The engineering properties associated with the individual layers were calculated using formulas from the mechanics of materials. These formulas were given in the book by Hyer [30]. The rule of mixtures result is used to calculate the fiber direction Young's modulus, E_1^C, and the in-plane Poisson's ratio, υ_{12}^C. The rule of mixtures uses the fiber and matrix volume fractions, ϕ^f and ϕ^m, and the appropriate constituent material properties. Here, the superscript, C, stands for "composite."

$$E_1^c = \phi_f E_1^f + \phi_m E^m \tag{6}$$

$$\upsilon_{12}^{c} = \phi_f \upsilon_{12}^{f} + \phi_m \upsilon^{m} \tag{7}$$

The modified rule of mixtures [30] is generally used in mechanics of materials for unidirectional lamina results for increased level of accuracy in estimation of the transverse extensional modulus. The inverse of the transverse layer modulus is given with respect to the fiber volume fraction, the transverse fiber modulus, and the matrix modulus as in Eq. 8.

$$\frac{1}{E_2^c} = \frac{1-\sqrt{\phi_f}}{E^m} + \frac{\sqrt{\phi_f}}{\sqrt{\phi_f}E_2^f + \left(1-\sqrt{\phi_f}\right)E^m} \tag{8}$$

Finally, the expression for in-plane shear modulus of a unidirectional layer used for mechanics of materials is taken from the concentric cylinders result [30]. The composite shear modulus, G_{12}^{C}, is given with respect to the matrix shear modulus, G_m, the fiber volume fraction and the fiber shear modulus, G_{12}^{f}.

$$G_{12}^{c} = G_m \left[\frac{\left(G^m + G_{12}^f\right) - \phi_f \left(G^m - G_{12}^f\right)}{\left(G^m + G_{12}^f\right) + \phi_f \left(G^m - G_{12}^f\right)} \right] \tag{9}$$

The mechanics of materials relations are used with the *in situ* pristine fiber and matrix constituent properties, found previously by the Helius Material Manager, to calculate unidirectional ply properties. CLT is then used to calculate idealized properties of a single woven layer using the stacking sequence that was mentioned above. These idealized properties are generally much higher than the expected properties of the corresponding woven ply. Since, the actual pristine properties of a woven ply are known, a "waviness factor", W, for each engineering property can be calculated as follows (for E_1 in this example) in Eq. 10.

$$W_{E_1} = \frac{E_1^{\text{actual}}}{E_1^{\text{CLT}}} \tag{10}$$

Here, E_1^{actual}, is the lamina extensional modulus determined by the appropriate ASTM test standard and available in published literature, and E_1^{CLT}, is the idealized lamina extensional modulus calculated using the method outlined. Now, that this "waviness factor" has been determined, idealized versions of the damaged material properties for the matrix damaged element regions of the FEM, as well as the fiber damaged element regions of the FEM are next calculated using the CLT method, but this time using fiber and matrix constituent properties with the appropriate stiffness degradations (e.g. 90% reduction in matrix stiffness and 99% reduction in fiber stiffness for the

region associated with fiber cracking in the FEM). The "waviness factor" is then used to calculate more appropriate degraded properties as follows in Eq. 11 for the damaged Young's modulus in the fill tow direction. Here, E_1^{idealdam} is the idealized damaged Young's modulus calculated from CLT.

$$E_1^{\text{dam}} = W_{E_1} E_1^{\text{idealdam}} \tag{11}$$

The damaged warp modulus, E_2^{dam}, and the damaged in-plane shear modulus, G_{12}^{dam}, are calculated in the same fashion. The Poisson's ratios are not degraded from the values used from literature. The out-of-plane Young's modulus, E_3^{dam}, is assumed to degrade from the values used from literature by the same amount calculated for the fill modulus. Additionally, the calculated degradation of the in-plane shear modulus is applied to the other two shear moduli required for the fully orthotropic engineering property definition of the damaged facesheet plies. These methods are useful for estimating the damaged material properties needed in the present research, although the assumptions used must be taken into account as sources of uncertainty.

III. CAI Analysis Results

A new FEM for the CAI analysis of thin-facesheet honeycomb core sandwich panels with low velocity impact damage has been developed. The two major advantages of the new model include the incorporation of a progressive failure analysis for damage propagation in the facesheets, and a detailed representation of the impact damage included in the model prior to the CAI analysis. The former's importance is two-fold. First, a more accurate representation of the indentation propagation failure mode can be achieved. Second, the new FEM has the ability to represent multiple failure modes, to include the crack propagation failure mode of the high density honeycomb core materials found during the current research. The detailed impact damage representation also adds fidelity to the model to provide improved accuracy in analysis results.

The purpose of the following section is to validate the new FEM by comparing analysis results with experimental test results. In Part 1 [1] of the current research, tests were completed on two nearly identical honeycomb core sandwich panel material systems. They differed only in the density of the Nomex honeycomb core included in their construction, and were given the designations, 3PCF-XX and 6PCF-XX, to differentiate them in this regard. A total of 24 test coupons were

damaged with a low velocity impact and tested to CAI failure. The impact damage in each of these test coupons was considered using non-destructive evaluation (NDE) techniques. This data, combined with some data taken using dissection of impact survey coupons, was used to create 24 total analysis models. The analysis predictions will be compared with experimental results, time lapse images, and digital image correlation (DIC) measurements.

A. 3PCF-XX Analysis Results

In the following section, the CAI analysis results for 3PCF-XX series test specimens will be compared with experimental test results for these panels. For the 3PCF-XX series CAI tests, a total of twelve coupons were tested to failure. Low velocity impact damage was inflicted on each of these test coupons, prior to compressive loading. Three coupons were impacted at each of the following four energy levels: 1.0, 3.0, 5.0 and 7.0 ft-lb. An analysis of each coupon has been completed using the unique FEM developed here with the inputs from observations and measurements made on experimental test coupons.

Due to symmetry, each 3PCF-XX FEM represents a 2.75 in. by 2.75 in. quadrant of a 3PCF-XX test coupon. The 0.02 in. thick facesheets consisted of woven S2-glass plies, and the core was a 0.75 in. thick 3 lb/ft^3 Nomex honeycomb. Additional material details can be found in the Part 1 report. The elastic facesheet material properties used in the analyses are summarized in Table 1. The lamina material properties are similar to the experimental properties given by the National Institute of Aerospace Research (NIAR) [31], though they differ slightly due to processing by the Helius Material Manager. The matrix and fiber constituent properties are the *in situ* properties calculated by the Material Manager. The material strengths used can be found in Table 2 for the S2-glass/epoxy facesheets, which includes the knee strengths for matrix failure prediction, which are set at 85% of the lamina strengths. The material strengths are based on the NIAR data [31], except the in-plane shear strength which was artificially increased to prohibit unrealistic matrix failure during analysis in the 45 degree plies. (It can also be noted that the experimental test results for in-plane shear, which can be obtained by contacting the NIAR test engineers, do not exhibit a true failure point. The engineers stop the test prior to failure once 5% strain was reached.)

The material properties used in the continuum representation of the Nomex honeycomb are shown in Table 3. These material properties were either given by in the literature by Hexcel Corp. [32], or were calculated using the equations found in Gibson and Asby [13]. The out-of-plane compressive failure strength, the peak compressive stress in Fig. 3, was 270 psi [32]and the corresponding compressive failure strain for the Nomex honeycomb was 0.0135 in/in. Each analysis was displacement controlled, as in the experimental testing described in Part 1 of the research.

Table 1 S2-glass/Epoxy woven fabric lamina material properties used in the FEM.

S2-glass Lamina	E_1 (Msi)	E_2 (Msi)	E_3 (Msi)	ν_{12}	ν_{13}	ν_{23}	G_{12} (Msi)	G_{13} (Msi)	G_{23} (Msi)
	4.622	4.527	1.287	0.109	0.361	0.362	0.613	0.385	0.385
Fiber Constants	E_1 (Msi)	E_2 (Msi)	E_3 (Msi)	ν_{12}	ν_{13}	ν_{23}	G_{12} (Msi)	G_{13} (Msi)	G_{23} (Msi)
	15.70	11.59	11.59	0.254	0.254	0.201	6.656	6.656	4.825
Matrix Constants	E_1 (Msi)	E_2 (Msi)	E_3 (Msi)	ν_{12}	ν_{13}	ν_{23}	G_{12} (Msi)	G_{13} (Msi)	G_{23} (Msi)
	0.466	0.466	0.466	0.331	0.331	0.331	0.175	0.175	0.175

Table 2 S2-glass/Epoxy woven fabric laminate strengths used in the FEM.

Lamina Strengths	$^{(+)}S_{11}$ (ksi)	$^{(-)}S_{11}$ (ksi)	$^{(+)}S_{22}$ (ksi)	$^{(-)}S_{22}$ (ksi)	$^{(+)}S_{33}$ (ksi)	$^{(-)}S_{33}$ (ksi)	S_{12} (ksi)	S_{13} (ksi)	S_{23} (ksi)
	79.92	-69.07	79.92	-69.07	79.92	-69.07	15.00	0.00	0.00
Knee Strengths	Tensile (ksi)		Compressive (ksi)		In-plane Shear (ksi)				
	67.93		-58.71		13.00				

Table 3 3 lb/ft^3. Nomex honeycomb core orthotropic engineering constants used in the FEM.

3PCF Core	E_1 (ksi)	E_2 (ksi)	E_3 (ksi)	ν_{12}	ν_{13}	ν_{23}	G_{12} (ksi)	G_{13} (ksi)	G_{23} (ksi)
	0.500	0.500	20.0	0.500	0.000	0.000	0.125	4.50	2.50

Damage incorporated into the model to simulate the low velocity impact damage was described, previously. The dent depth and diameter definition was taken from the actual experimental measurements of individual 3PCF-XX series CAI test coupon, prior to compressive loading. The inputs of damaged core region depth and diameter, as well as the damaged facesheet region diameter (and length for the fiber damaged region in highly damaged coupons), was taken from results of the drop tower impact survey of damage formation. Thus, models of test coupons impacted at the same im-

pact energy have identical inputs for these damage components. The numeric values which concern the geometry of the impact damage dent and the damaged material regions can be found in Table 4.

Table 4 FEM definition inputs for analysis of 3PCF-XX series test coupons.

FEM Coupon Name	Impact Energy Represented (ft-lb.)	Residual Dent Diameter (in.)	Residual Dent Depth (in.)	Damaged Core Region Diameter (in.)	Damaged Core Region Depth (in.)	Facesheet IFF Region Diameter (in.)	Facesheet Fiber Fracture Region Length (in.)
3PCF-01	3.0	0.917	0.0050	1.0612	0.1670	0.3360	Not Applicable
3PCF-02	1.0	0.633	0.0050	0.8695	0.1000	0.2790	Not Applicable
3PCF-03	3.0	1.033	0.0195	1.0612	0.1670	0.3360	Not Applicable
3PCF-05	1.0	0.717	0.0060	0.8695	0.1000	0.2790	Not Applicable
3PCF-07	7.0	1.300	0.2170	1.0922	0.2273	0.5910	0.458
3PCF-08	5.0	1.200	0.1500	1.0929	0.1570	0.5220	0.345
3PCF-09	7.0	1.400	0.1755	1.0922	0.2273	0.5910	0.458
3PCF-10	5.0	1.300	0.1195	1.0929	0.1570	0.5220	0.345
3PCF-12	5.0	1.283	0.1400	1.0929	0.1570	0.5220	0.345
3PCF-13	3.0	0.983	0.0190	1.0612	0.1670	0.3360	Not Applicable
3PCF-15	1.0	0.633	0.0045	0.8695	0.1000	0.2790	Not Applicable
3PCF-16	7.0	1.333	0.1820	1.0922	0.2273	0.5910	0.458

The three values which define the material property degradation in all analysis models are as follows.

1. The stiffness of "damaged" core element was reduced to 60% of the pristine properties.
2. The stiffness of the matrix constituent properties of "damaged" elements in the IFF region of the facesheet model was reduced to 10% of the pristine properties.
3. For the fiber fracture region in some analysis models, fiber properties are reduced to 1% of their pristine value in addition to the 90% reduction in matrix properties.

The indentation propagation failure mode was demonstrated for each of the 3PCF-XX analyses completed, as expected from experimental testing discussed in Part 1 of the current research [1]. The FEM representation of this failure mode is shown in Fig. 9, along with images from high speed camera photography, for comparison. The appropriate reaction force vs. applied displacement was also predicted in each analysis, where a sudden drop in reaction force is found at failure for each analysis performed [2].

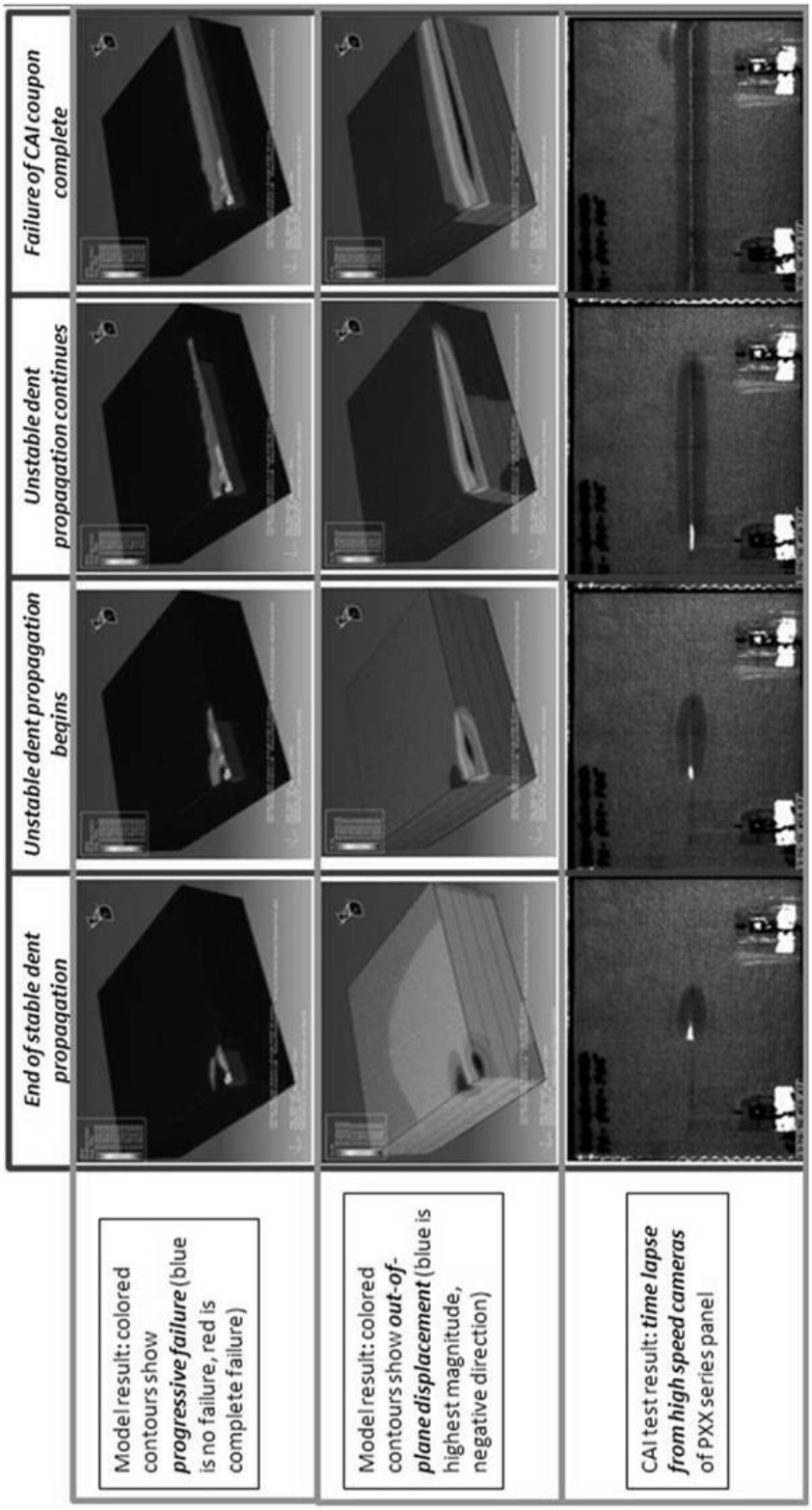

Fig. 9 Demonstration of indentation propagation failure mode prediction example, as seen in analysis of 3PCF-XX series coupons, with high speed camera experimental test results.

The comparison between experimental and analysis results presented here is focused on the CAI failure load. The comparison of these results is shown in Fig. 10, for the 3PCF-XX series specimens, though this comparison would be similar if shown for CAI failure load or CAI failure strain.

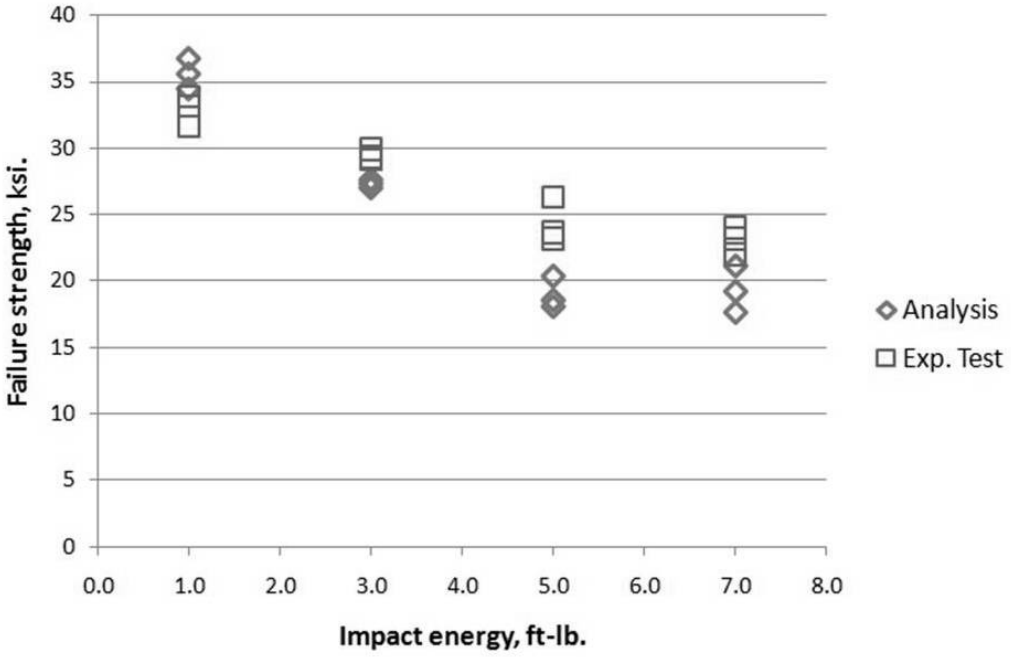

Fig. 10 3PCF-XX analysis results: comparison of predicted CAI failure strength to experimental test results.

Many of the 3PCF-XX analysis results show good agreement with experimental test results. The error ranged in magnitude from about 20% to less than a percent. Although the largest errors are significant, the analysis results are generally conservative, except for the test coupons with the lowest amounts of damage. The analysis results for failure strength approach a minimum, which is shown by comparison of the analysis results for the models with damage representing both 5.0 and 7.0 ft-lbs. energy level impacts. The failure stress result for each of these six analysis data points are similar.

A comparison can also be made between the stable dent growth predicted in the FEA and the stable dent growth measured using the DIC system. The DIC system was used for a select set of four 3PCF-XX series test coupons, and was discussed previously in Part 1 of the research. Results for the predicted indentation growth found during analysis were produced using the ABAQUS/Viewer

for these four test cases. One test case was considered at each of the four damage levels (1.0, 3.0, 5.0 and 7.0 ft-lbs.) The analysis predictions for the dent length measurements in the coupon width (x-) direction, coupon load (y-) direction, and the dent depth measurement in the through the thickness (z-) direction are shown in Figs. 11, 12, and 13, respectively, with comparison to the corresponding DIC measurements. In these figures, 100% of the failure load indicates the load just prior to failure.

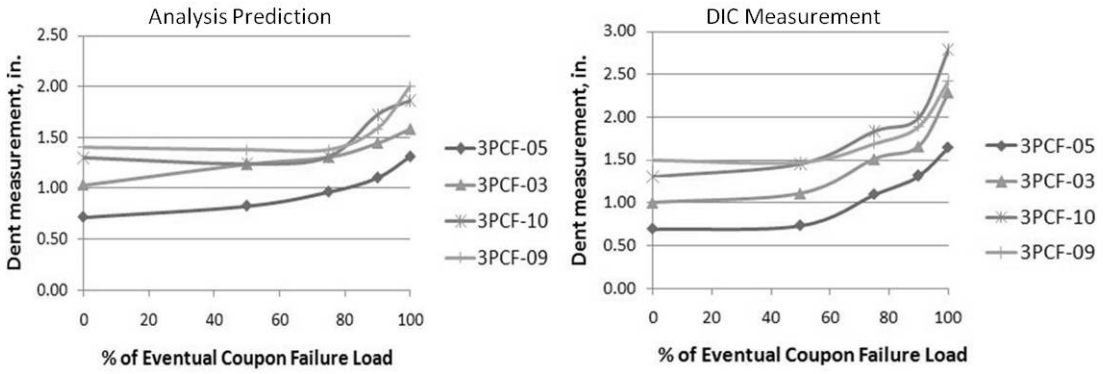

Fig. 11 Comparison of analysis predictions and DIC measurements for dent growth in the coupon width direction (x-direction) in 3PCF-XX CAI test coupons.

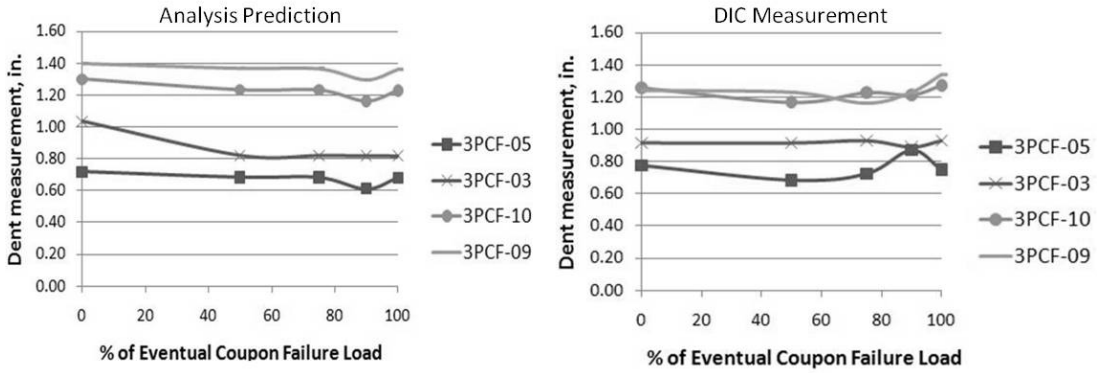

Fig. 12 Comparison of analysis predictions and DIC measurements for dent growth in the coupon load direction (y-direction) in 3PCF-XX CAI test coupons.

As expected from experimental testing, more growth is seen in the coupon width direction, than in the coupon load direction for the CAI analysis predictions. The stable dent growth predicted in the width direction is only slightly smaller than the measurements taken with the DIC system. However, the dent depth does not obtain the same amount of growth seen in DIC measurements of 3PCF-XX series experimental tests (Fig. 13). The dent depths found in analysis are about half the

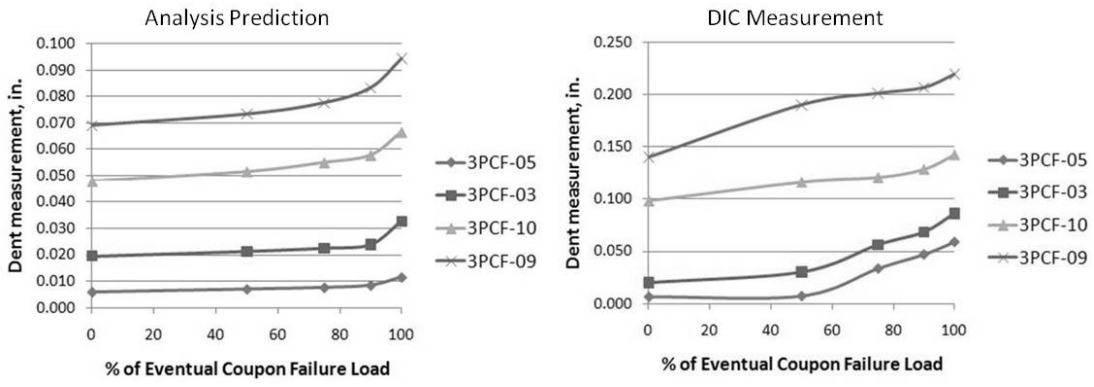

Fig. 13 Comparison of analysis predictions and DIC measurements for growth of the maximum dent depth (z-direction) in 3PCF-XX CAI test coupons.

size at failure as the corresponding measurements taken in experimental tests.

B. 6PCF-XX Analysis Results

The current section contains the analysis results for the higher density core, 6PCF-XX sandwich panels. A different failure mode, called crack propagation in the current research, was found to result from the presence of the high density honeycomb core. Like the 3PCF-XX series CAI tests, a total of twelve 6PCF-XX coupons were tested to failure. Low velocity impact damage was inflicted on these test coupons at each of the following four energy levels: 1.0, 3.0, 5.0 and 7.0 ft-lb.

The geometry of the 6PCX-XX test coupon models was identical to those described previously for the 3PCF-XX set. Complete details on the construction of these materials were given in Part 1 of present research. The elastic material properties used in the analyses were summarized in Table 1 for the S2-fiberglass/Epoxy facesheets, and the corresponding lamina strengths and knee strengths were given in Table 2. These values are similar to those available in the literature [31], but some differences were discussed in the previous section. The elastic material properties for the higher density, 6 lb/ft^3, honeycomb core are given in Table 5. These properties were either given by Hexcel Corp. [32], or were calculated using the relations found in Gibson and Ashby [13]. The out-of-plain compressive failure stress for the higher density core, which corresponds to the peak compressive stress seen in a curve similar to that shown in Fig. 3, was 925 psi [32], and the corresponding compressive strain value was 0.0154 in/in. Each analysis was, again, displacement controlled.

Table 5 6 lb/ft^3. Nomex honeycomb core orthotropic engineering constants used in the FEA.

	E_1 (ksi)	E_2 (ksi)	E_3 (ksi)	ν_{12}	ν_{13}	ν_{23}	G_{12} (ksi)	G_{13} (ksi)	G_{23} (ksi)
6PCF Core	1.500	1.500	60.0	0.500	0.000	0.000	0.375	13.00	6.50

The components of impact damage used to define the geometry of "damaged" regions of the model and the appropriate material properties were described previously. The numeric values which govern the geometry of the impact damage dent and the damaged material regions in the 6PCF-XX analysis models can be found in Table 6. The three values which define the material property degradation in all analysis models are as follows, and are identical to those used in 3PCF-XX series analyses:

1. The stiffness of "damaged" core element was reduced to 60% of the pristine properties.
2. The stiffness of the matrix constituent properties of "damaged" elements in the IFF region of the facesheet model was reduced to 10% of the pristine properties.
3. For the fiber fracture region in some analysis models, fiber properties was reduced to 1% of their pristine value in addition to the reduction in matrix properties.

Table 6 FEM definition inputs for analyses of 6PCF-XX series test coupons.

FEM Coupon Name	Energy Represented (ft-lb.)	Dent Diameter (in.)	Residual Dent Depth (in.)	Damaged Core Region Diameter (in.)	Damaged Core Region Depth (in.)	Facesheet IFF Region Diameter (in.)	Facesheet Fiber Fracture Region Length (in.)
6PCF-01	7.0	1.000	0.1605	0.8595	0.1999	0.6010	0.498
6PCF-02	3.0	0.783	0.0155	0.7738	0.1791	0.4970	Not Applicable
6PCF-03	5.0	0.833	0.1220	0.8200	0.1415	0.5830	0.493
6PCF-06	5.0	0.917	0.1190	0.8200	0.1415	0.5830	0.493
6PCF-07	1.0	0.583	0.0060	0.6718	0.1088	0.4440	Not Applicable
6PCF-09	3.0	0.633	0.0170	0.7738	0.1791	0.4970	Not Applicable
6PCF-10	1.0	0.517	0.0055	0.6718	0.1088	0.4440	Not Applicable
6PCF-11	7.0	0.900	0.1560	0.8595	0.1999	0.6010	0.498
6PCF-12	5.0	0.867	0.1080	0.8200	0.1415	0.5830	0.493
6PCF-14	7.0	1.000	0.1590	0.8595	0.1999	0.6010	0.498
6PCF-15	3.0	0.800	0.0185	0.7738	0.1791	0.4970	Not Applicable
6PCF-16	1.0	0.583	0.0060	0.6718	0.1088	0.4440	Not Applicable

The 6PCF-XX materials were of particular interest during analysis, because one of the principal contributions of the current research is the implementation of PFA of the facesheets. This inclu-

sion gives the model the unique ability to predict a new failure mode, crack propagation. Using Helius:MCT, the new model is successful at capturing this failure mode in all 6PCF-XX samdwich panels, as shown in Fig. 14. The unstable crack propagation for an example test coupon in the FEA analysis is compared to a sequence of photos from high speed photography of an experimental test. Model results for out-of-plane displacement shows that no local buckling is predicted, and there is very little dent growth during the analysis. FEA results for element damage predict the facesheet crack which appears in experimental results.

The point of sudden drop in coupon reaction force in the FEA results for force vs. displacement indicates the point of global coupon failure for identifying CAI strength. The main focus of the comparison between the analysis results and the experimental test results will again be CAI strength. However, results can also be obtained from FEA for failure load, and failure strain, and these analysis results would compare to experimental test results in a similar manner. The results comparison is shown in Fig. 15.

The FEA results of the 6PCF-XX series test coupons tended to be non-conservative. Numerically, the prediction errors varied from about 20% to less than a percent, as in the 3PCF-XX analyses. Only a few of the results were in error by 20%; however, most were under 15%. There does not appear to be any correlation between the accuracy of the model for a specific analysis result and the damage level of the test coupon. It is interesting to note that in the analysis predictions, there is very little spread in the CAI failure results for a given impact damage level, though the impact damage inputs do vary. This is in contrast to the large amount of variation in the experimental CAI test results found at a certain impact energy level. Since, only the dent depth and diameter varied with each analysis and the remaining inputs were kept constant (since they came from the 6PCF-XX impact survey specimen and not the actual CAI test specimen), one can expect little variation in the analysis prediction results.

A comparison was again made between analysis predictions for indentation growth and experimental test measurements of select 6PCF-XX series test coupons using the DIC system. Analysis prediction results for dent size in the coupon width and load directions, and the maximum dent depth can be seen in Fig. 16, 17 and 18, respectively, with comparisons to the DIC measurements.

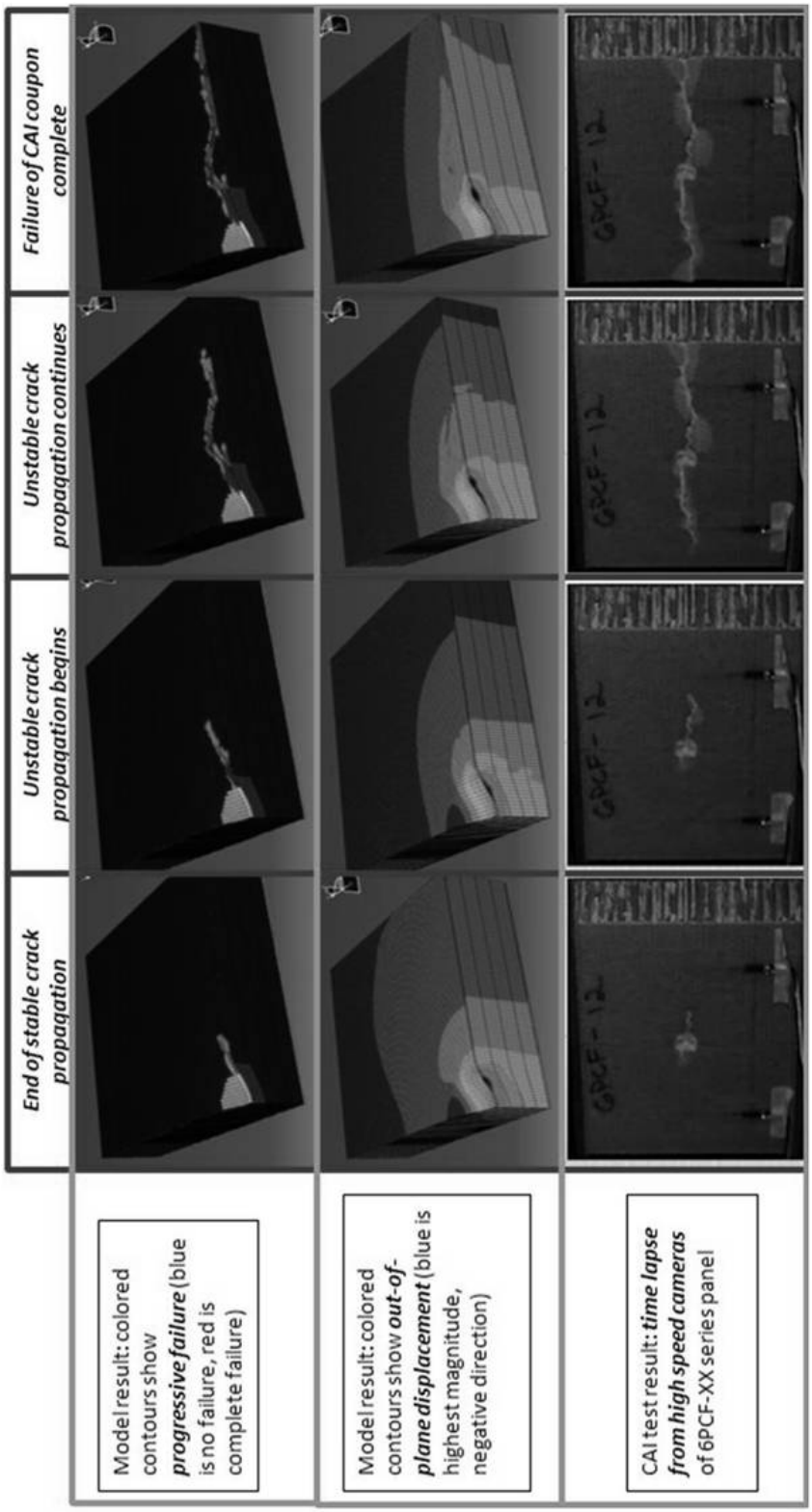

Fig. 14 Demonstration of crack propagation failure mode prediction example, as seen in analysis of 6PCF-XX series coupons.

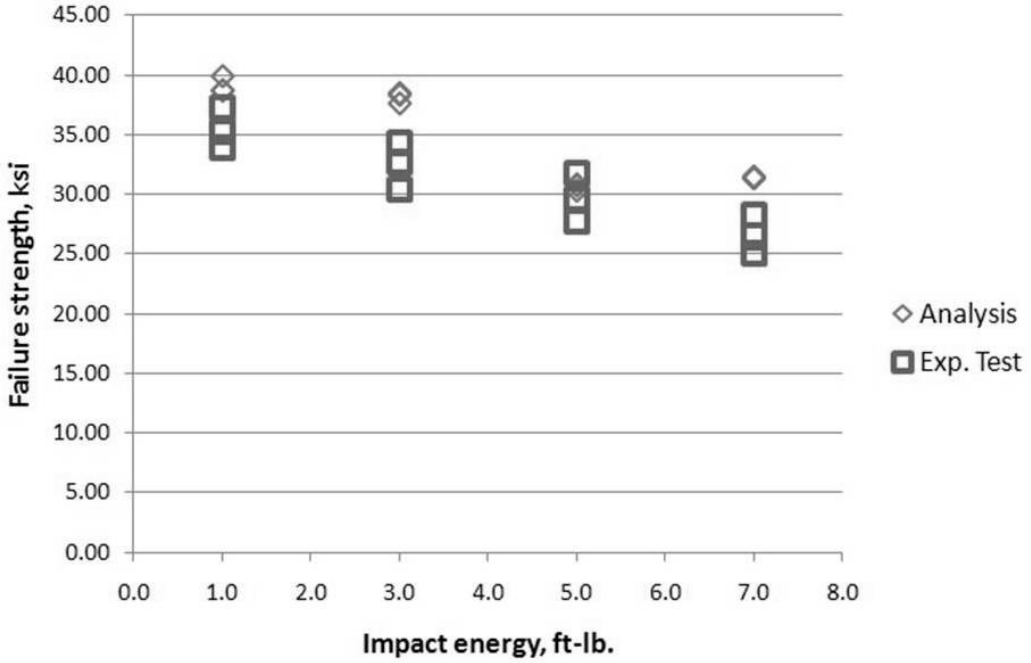

Fig. 15 6PCF-XX analysis results: comparison of predicted CAI failure strength to experimental test results.

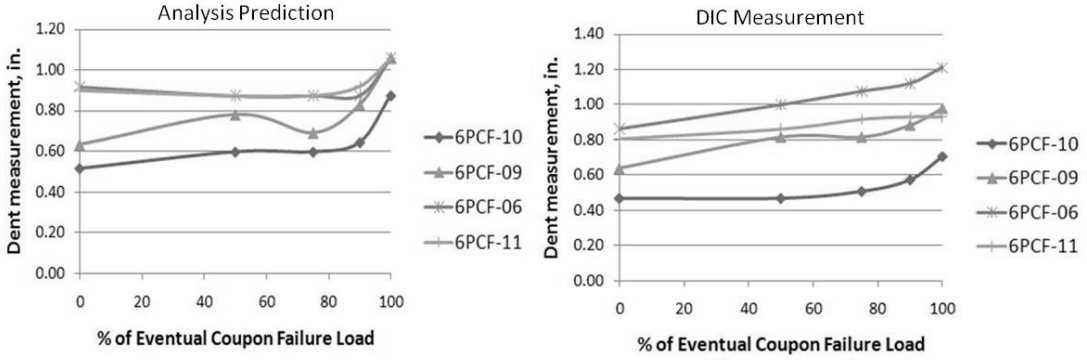

Fig. 16 Comparison of analysis predictions and DIC measurements for dent growth in the coupon width direction (x-direction) in 6PCF-XX CAI test coupons.

There was little predicted growth of the residual dent during the FEA of 6PCF-XX series test coupons. This was expected from the experimental test results. Some growth is predicted at the very last stage of the coupon response in the coupon width direction, shown in Fig. 16. These results compare well to the experimental test results shown in Part 1 of the current research [1]. The correlation between the experimental test results and the FEA predictions is better for the 6PCF-XX series materials, than it was for the 3PCF-XX series materials.

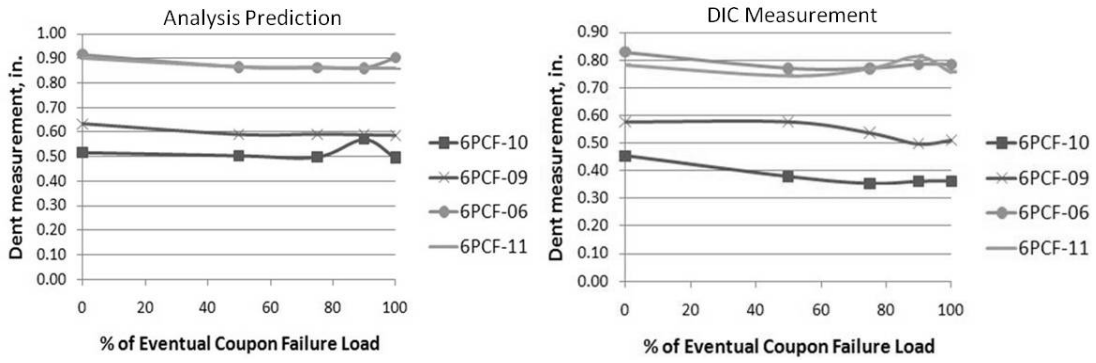

Fig. 17 Comparison of analysis predictions and DIC measurements for dent growth in the coupon load direction (y-direction) in 6PCF-XX CAI test coupons.

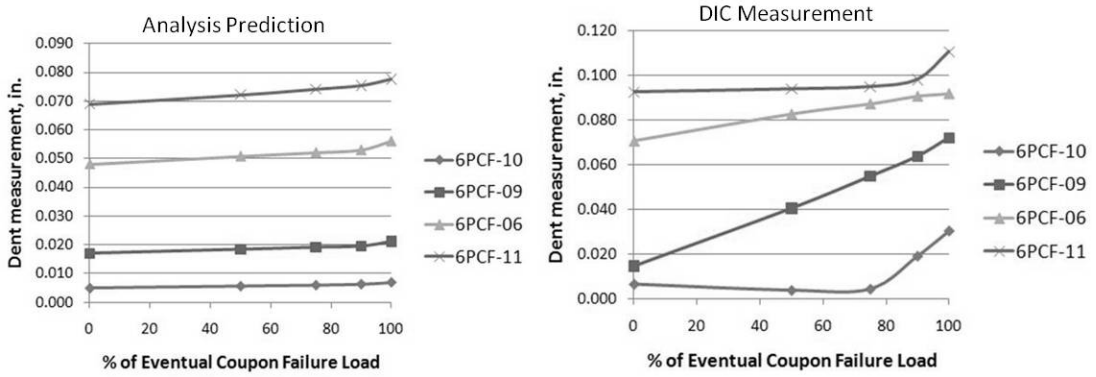

Fig. 18 Comparison of analysis predictions and DIC measurements for growth of the maximum dent depth (z-direction) in 6PCF-XX CAI test coupons.

C. Parametric Study of Core Density

One of the major conclusions of the present research is that there is a dependence of the CAI failure mode in the sandwich panels studied on the density of the honeycomb core material. In the present study, the traditional sandwich panel CAI failure mode, indentation propagation, is found for panels with the lower density 3 lb/ft^3 honeycomb core. The higher density, 6 lb/ft^3, core clearly produced a different failure mode, crack propagation, and higher failure strengths. As a result, a parametric study has been completed to determine the critical density of the honeycomb core at which the failure mode transitions from indentation propagation to crack propagation failure mode. In addition, one of the purposes of this study was to determine the increase in failure strength possible by increasing the core density, without changing any of the other parameters. The material

properties which define the crush response of the various density Nomex honeycomb cores will be discussed, and subsequently, the results of the parametric study analyses will be presented.

A single CAI model was chosen to determine the effect of the core density on the CAI response. For the parametric study, the geometry modeled corresponds to the 3PCF-XX and 6PCF-XX test coupons, so that a single 2.75 in. by 2.75 in. quadrant of a test coupon is modeled with 0.02 in. thick facesheets and a 0.75 in. thick core. Damage in each model used with the parametric study was modeled using the inputs for the 3PCF-13 test coupon, which were given previously in Table 4. The stiffness reductions for the damaged core, IFF damaged facesheet, and fiber fracture damaged facesheet regions' stiffness reductions are as follows:

1. The stiffness of "damaged" core element was reduced to 60% of the pristine properties.

2. The matrix constituent stiffness reduction was 90% in the IFF regions of the facesheet model.

3. The fiber constituent reduction was 99% and the matrix constituent stiffness reduction was 90% when fiber fracture is predicted in the PFA.

It was noted in the experimental test results discussed in Part 1 of the current research [1], that the core density will have a small, but noticeable effect on damage formation in the sandwich panel. However, the damage was kept constant for the parametric study so that the honeycomb core properties are the only variable which can change the analysis results. The results of this study can be thought of as conservative, since impact damage was shown to decrease in size with increased core density.

The sandwich core is a hexagonal cell Nomex honeycomb with 0.125 in. cell size. Commercially available Hexcel material property data lists core crush and plate shear data for this type of honeycomb at a variety of nominal densities, including the 3 and 6 lb/ft^3 densities, which were primarily studied in the present research. The values for the core crush strength and modulus, for each density Nomex honeycomb core listed in the available data [32], is shown in Figs. 19 and 20, respectively.

A linear relationship was found based on a regression fit of this data. The linear relationships calculated in the present research for the core crush strength and linear elastic modulus are given

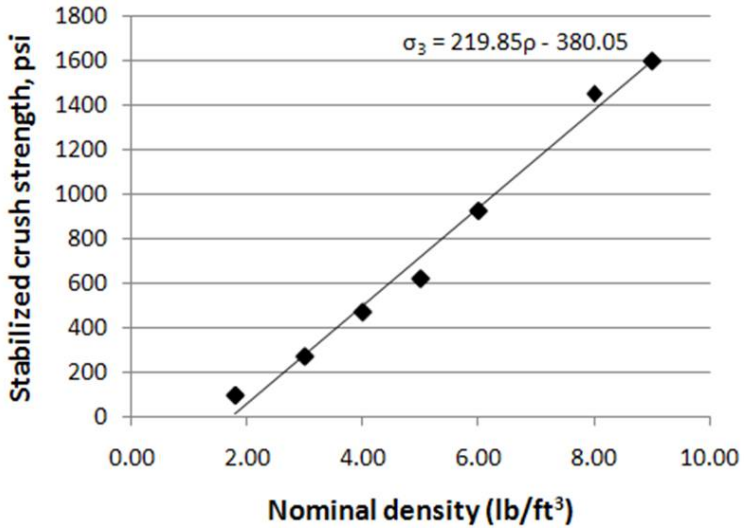

Fig. 19 Core crush strength of Nomex honeycomb shown varying with nominal core density, and the data fit calculated for use with the parametric study analyses.

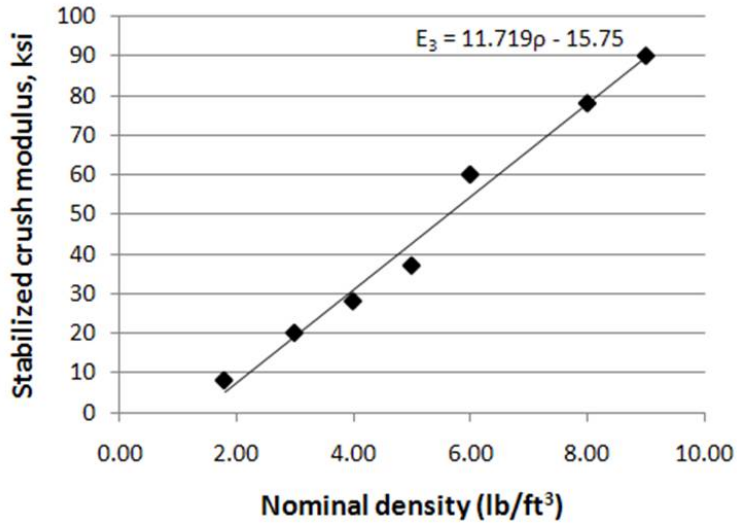

Fig. 20 Core out-of-plane modulus of Nomex honeycomb shown varying with nominal core density, and the data fit calculated for use with the parametric study analyses.

in Figs. 19 and 20, respectively. The in-plane shear properties necessary were found similarly. Other properties necessary, including the in-plane extensional moduli, were calculated using the relationships given in Gibson and Ashby [13]. The parametric study was completed with continuum core models representative of honeycomb core densities ranging from 3 to 6 lb/ft^3, with a step size of 0.5 lb/ft^3. The bounds on the honeycomb core density were chosen so that both indentation propagation and crack propagation failure modes would be represented in the parametric study

results.

The results of the parametric study clearly show the usefulness of a CAI model which can handle multiple failure modes. After each of the seven analyses was completed, both failure modes were represented in the parametric study. The failure strength was predicted for each honeycomb core density uesd in the analyses completed. The predicted failure strength vs. core density is shown in Fig. 21. The type of failure mode is indicated by the symbol used for a particular data point.

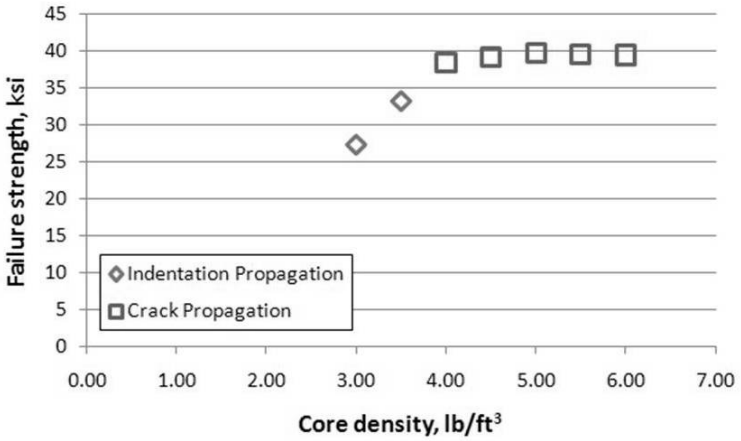

Fig. 21 Parametric study results: failure strength vs. nominal core density associated with continuum core properties.

From the results in Fig. 21, the following two conclusions can be made. First, the failure strength of the sandwich panel test coupon increases with honeycomb core density when the failure mode is indentation propagation. Second, at a given honeycomb core density, the failure mode will transition from indentation propagation to crack propagation as the density is increased. This is clearly seen to occur near the 4 lb/ft^3 core density level. It can also be seen that the failure strength has reached a maximum once the failure mode changes to crack propagation. This suggests that a trivial mass penalty could be added to the sandwich panel to obtain a significant strength increase. The predicted strength increase vs. the calculated mass penalty is considered in Fig. 22.

The increase in failure strength in Fig. 22 is calculated as a percentage of the 3 lb/ft^3 failure strength. The mass of the test coupon model is normalized with respect to the complete sandwich panel structure, which includes both the facesheets and the core. The increase in mass is due only to the increase in core density, but is shown as a percentage of the complete panel mass. The strength

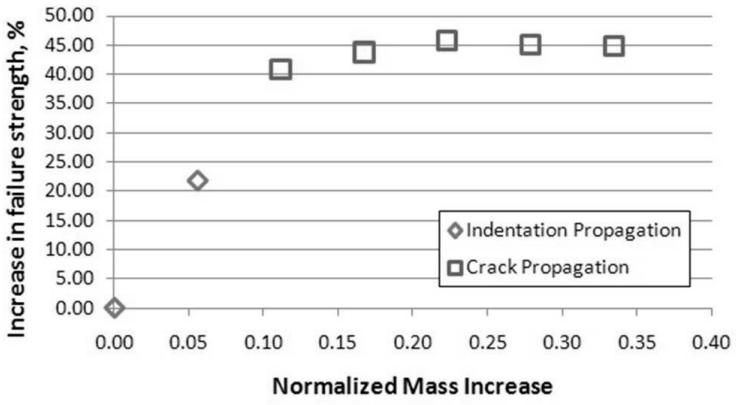

Fig. 22 Parametric study results: percentage strength increase vs. normalized mass increase.

increase is a maximum once the failure mode has transitioned from indentation propagation to crack propagation. With respect to the data point representing the 4 lb/ft^3 case, a strength increase of just over 40% was achieved for only a 10% weight penalty. Since the CAI strength of a composite material is typically one of the most conservative strength estimates, this predicted strength increase is very significant!

IV. Conclusions

Composite sandwich structures are increasingly being considered in the design of tomorrow's aerospace vehicles. One of the major design challenges in composites is the understanding of damage formation and response of a composite structure with damage present. Composite sandwich structure response to compression after low velocity impact has been the subject of the present research, which has included both experimental testing and finite element analysis (FEA). The current paper, Part 2, of the present research, has focused on the model development and analysis.

The current state of compression after impact (CAI) analysis was briefly described. Important areas of improvement which are needed were identified to include: a facesheet PFA, increased damage realism, and increased experimental validation. A new model which seeks to make improvements in these areas has been developed. The new model includes an implementation of MCT failure theory using the commercially available software, Helius:MCT, by Firehole Composites. A successful implementation of PFA is absent from previous CAI models found in the literature, so CAI analysis

with this capability is concluded to be the first of its kind. The new FEM model has the ability to successfully model and predict multiple failure modes, including the two modes found in the experimental work presented in the present study: indentation propagation and crack propagation. The new model's results demonstrate high-fidelity physics based representations of both failure modes.

The new CAI model was used to analyze the CAI response of each of the 32 coupons tested to failure during experimental work. Results were given for failure stress. Specific consideration was given to analysis results for coupon failure strength for comparison to experimental test results, but any of the global failure measurements could have been used. The new model showed similar error to other currently available CAI models for some of the analyses when compared to experiments. However, for most of the results, the resulting error was lower, and for some results, the error was significantly low. Analysis results which were obtained for the current research are acceptable, but further confidence could be gained by increasing damage observation accuracy.

The final result discussed in the present work was a parametric study on the effect of core density on sandwich panel CAI response. This result clearly showed that increasing the specimen's core density will change the failure mode from indentation propagation to crack propagation. In addition, CAI failure strength was increased with the core density increase, until the failure mode changed to crack propagation. The parametric study results showed that a substantially large CAI strength increase could be obtained for only a small increase in mass. This result demonstrates the new abilities of the new model for CAI analysis, as well as its benefit to engineering design.

Appendix

The large amount of CAI test data generated in the experimental portion, Part 1 [1], of the current research, meant that increased impact damage detail could be included in the FEM. Many of these details were used as inputs into a MATLAB program which created the ABAQUS input file used in these analyses. The following section will describe how each detail affects the overall model results for CAI analysis. The purpose of this study is to identify the maturity level associated with various aspects of the model. Some aspects of the model are identified as areas of necessary

improvement for future CAI model development, or use of the current model in an engineering design problem. The following inputs must be used to define the damage, as discussed in the preceeding section:

1. Residual dent depth
2. Residual dent diameter
3. Core damage depth
4. Core damage diameter
5. Core damage material property degradation
6. Matrix damaged (inter-fiber fracture or IFF) facesheet region diameter
7. Fiber and matrix damaged facesheet region length
8. Matrix material property degradation
9. Fiber material property degradation

The majority of these inputs are the result of explicit measurements taken during experimental testing, and have low levels of uncertainty associated with them. The following section will describe these inputs, which include the residual dent's diameter, the residual dent's maximum depth, the core damage region's diameter, the facesheet's IFF region's diameter, and the facesheet's fiber fracture region's length (only used in models of highly damaged test coupons). In addition, each of these measurements is applied to the corresponding model input parameter using a level of precision close to the precision the measurement was taken with.

One additional input, taken from explicit measurement of a given test coupon, is the depth of the impact damaged core region of the model. Unfortunately, due to the mesh pattern and density used, the application of this measurement to the FEM is done with reduced precision. The possible effect of this uncertainty on the CAI analysis results is discussed in its own section. Finally, the last three model inputs discussed are the stiffness reductions given to the material properties associated with damage in the model's core and facesheet regions. These three inputs were taken from various

sources, and are not experimental test measurements. The unique uncertainty they add to the model will be discussed in the third sensitivity study subsection which follows.

A. Sensitivity to Impact Damage Definition

This section will describe the sensitivity of the new CAI model to the following MATLAB function inputs: the residual dent's diameter, the residual dent's maximum depth, the core damage region's diameter, the facesheet's IFF region's diameter, and the facesheet's fiber fracture region's length. Four test coupon models were used in these sensitivity studies: 3PCF-02, 3PCF-16, 6PCF-07, and 6PCF-14. These models were specifically chosen for the following reasons. Two panels were chosen from material systems expected to fail at each of the two CAI failure modes discussed in the current research: indentation propagation (3PCF-XX), and crack propagation (6PCF-XX). This will allow the sensitivity of the model for these inputs to be tested for each specific failure mode. For each of these two material systems, a lightly damaged test coupon was studied (3PCF-02 and 6PCF-07), as well as a highly damaged test coupon (3PCF-16 and 6PCF-14). This will allow the sensitivity of the model to various initial levels of damage to be determined.

Each sensitivity study was conducted for one specific input, while the remaining inputs were kept constant. The nominal inputs for each of the four test cases used in the sensitivity studies are given in Table 7 below. The effect of an uncertainty of +/-15% with respect to each of the model inputs was considered. This level of uncertainty is very large with relation to the actual precision associated with the measurements of the inputs studied; however, some inputs will have larger effect on the model then others. This large level was chosen so that some change could be seen in each of the analyses completed. Since the change in each inputs was the same, each of the inputs discussed in the current section could be directly compared and ranked based on sensitivity.

A specific example is chosen to explain the process used to study model sensitivity to each input. The sensitivity of the FEM to the measurement of the residual dent depth of the 3PCF-02 test coupon will be used for this example. The measured dent depth of this particular test coupon was 0.005 in. using a dial caliper, which had a tolerance of 0.001 in. An uncertainty of +/-15% was studied, so that two analyses were completed. With all other model definition inputs left at

Table 7 Nominal input values used during the sensitivity studies to define the FEM.

MATLAB Function Input	3PCF-02 (in. or %)	3PCF-16 (in. or %)	6PCF-07 (in. or %)	6PCF-14 (in. or %)
Residual Dent Depth	0.0050	0.1820	0.0060	0.1590
Residual Dent Diameter	0.633	1.333	0.583	1.000
Core Damage Region Depth	0.1000	0.1820	0.1088	0.1999
Core Damage Region Diameter	0.8695	1.0922	0.6718	0.8595
Core Damage Stiffness Reduction	40%	40%	40%	40%
Facesheet IFF Region Diameter	0.279	0.591	0.444	0.601
Facesheet Fiber Fracture Region Length	Not Applicable	0.458	Not Applicable	0.498
Facesheet Damaged Matrix Stiffness Reduction	90%	90%	90%	90%
Facesheet Damaged Fiber Stiffness Reduction	99%	99%	99%	99%

their nominal values, an analysis was completed of the 3PCF-02 coupon with a conservative dent depth value of 0.00575 in. and a non-conservative value of 0.00425 in. Each of the two cases was considered for their effect on coupon CAI failure. The global failure of the the test coupon can be discussed with respect to failure load, failure stress, and failure strain. For this example all three will be discussed, and it will be shown that the results are very similar. Thus, for the results thereafter, only coupon failure load will be used.

The sensitivity study results for the example problem are shown in Table 8. The failure load, failure stress, and failure strain for both the non-conservative and conservative analyses are shown. The average of the two results is also given. Finally, the percent change from this average for either a 15% conservative or non-conservative estimate of the input studied is given. This information was gathered for each of the inputs considered in the current section. For each test case, the sensitivity of the model to each input could then be ranked from most sensitive to least sensitive. Thus, the importance of each input to the overall CAI analysis result can be shown.

The overall results of the study of the sensitivity of the CAI model to the MATLAB function inputs of the residual dent's diameter, the residual dent's maximum depth, the core damage region's diameter, the facesheet's IFF region's diameter, and the facesheet's fiber fracture region's length are shown in Table 9. For the lightly damaged coupons, which do not include the fiber fracture region, the sensitivity is ranked from 1 (most) to 4 (least sensitive). For the highly damaged coupons, which

Table 8 Example sensitivity study: effect of residual dent maximum depth definition on the predicted CAI failure of the 3PCF-02 test coupon model.

		Conservative Dent Depth	Non-conservative Dent Depth
3PCF-02	Failure Load (lbs)	7666	8142
	Average (lbs.)	7904	
	% +/- Average	3.01	
	Failure Stress (ksi)	34.85	37.01
	Average (ksi.)	35.93	
	% +/- Average	3.01	
	Failure Strain (μ-in/in)	9803	10401
	Average (μ-in/in)	10102	
	% +/- Average	2.96	

include a fiber fracture region, the ranking is from 1 to 5.

Table 9 Sensitivity study results for various MATLAB function inputs.

Panel	Input	Percent	Rank
3PCF-02	Dent depth	3.01	1
	Dent diameter	2.26	2
	Damaged facesheet diameter	0.92	3
	Core damage diameter	0.08	4
Panel	**Input**	**Percent**	**Rank**
3PCF-16	Dent diameter	16.40	1
	Core damage diameter	11.00	2
	Dent depth	5.32	3
	Crack length	0.86	4
	Damaged facesheet diameter	0.20	5
Panel	**Input**	**Percent**	**Rank**
6PCF-07	Damaged facesheet diameter	1.08	1
	Dent diameter	0.86	2
	Dent depth	0.64	3
	Core damage diameter	0.45	4
Panel	**Input**	**Percent**	**Rank**
6PCF-14	Dent diameter	2.68	1
	Damaged facesheet diameter	1.98	2
	Dent depth	1.39	3
	Core damage diameter	1.07	4
	Crack length	0.45	5

The sensitivity of the model to a relatively large uncertainty (+/-15%) was surprisingly small for most test cases. Except for two studies, the model sensitivity was 5% or less. For most of the inputs used for each of the four test cases, the sensitivity was less than 2%. The exceptions were the 3PCF-16 model's sensitivity to dent diameter and core damage diameter inputs. Fortunately, for both of

these inputs, the actual uncertainty associated with the measurements is much smaller than the uncertainty studied. The experimental measurements for these two inputs, shown in Table 7, were about 1 in. Thus, the uncertainty studied (15%) meant that the conservative and non-conservative estimates varied from the nominal value by about 0.15 in. The experimental uncertainty associated with these measurements can be estimated as $1/60^{\text{th}}$ of an inch for the dent diameter, and is less than 0.001 in. for the core damage region diameter. Therefore, since the actual uncertainty associated with these two measurements is much smaller, the uncertainty in the model results would actually be much smaller.

A few other interesting trends can be seen in the results. First, the measurement of the dent diameter has a relatively significant effect on all cases considered. Thus, it is important that this input is accurate. Additionally, the test cases which can be expected to fail by crack propagation (6PCF-XX) had very little sensitivity to changes in the core damage region's size. This can be expected since core damage primarily impacted out-of-plane deformation of the test coupons, which is already very small during the crack propagation failure mode. Finally, each input considered in the current section was shown to have some effect on the model results. So, it can be concluded that each of these inputs should be carefully considered in the CAI model.

B. Sensitivity to Core Damage Depth Definition

Special attention was given to the sizing of the core damage region's depth. This measurement, taken using the destructive evaluation of test coupons by optical microscopy, has a low uncertainty level. However, due to the low mesh density used, it cannot be implemented with the same precision. The sensitivity of the FEM analysis results was studied using the test cases described previously: 3PCF-02, 3PCF-16, 6PCF-07, and 6PCF-14. The measurements used as input for the depth of the core damage for each of these cases can be found in Table 7. The FEM was created in such a way as to define the core damage region's depth to the nearest element. The mesh was defined with eight elements through the core thickness. The sensitivity was studied with respect to a change in core damage region depth of +/- one element, since this is the possible error. The results of this portion of the sensitivity studies are shown in Table 10. The global coupon CAI failure load was again used

as the primary indication of sensitivity.

Table 10 Sensitivity study results, core damage region depth input.

	% Change in Failure Load
3PCF-03	5.39
3PCF-16	0.2
6PCF-07	0.938
6PCF-14	0.979

Remarkably, the change in CAI failure load associated with the core damage region's depth was small for three of the four test cases. For both crack propagation cases (6PCF-07 and 6PCF-14), the percent change for each case was just less than 1%. Of course, it should be expected that this input will have less effect on the crack propagation failure mode, than for the indentation propagation failure mode. This is due to the fact that the level of core damage present in the model will primarily affect the amount of out-of-plane deformation near the damage, which has been mentioned previously. However, for the highly damaged low density core test case (3PCF-16), the percent change was even smaller. For the lightly damaged case, 3PCF-02, the percent change was the largest, but this was mostly due to the lack of core damage in the non-conservative case (minus one element meant no damaged core elements were used). This result suggests that the depth of core damage is less important; however, it is important that at least some finite core damage depth is used.

C. Sensitivity to Element Stiffness Degradation

The final portion of the sensitivity study investigated the degradation in stiffness from pristine material properties which are incorporated in the elements within the "damaged" regions of the FEM. The three damaged regions in the models have been previously described, and include a damaged core region, and two damaged facesheet regions. The principal damaged facesheet region represents a region of inter-fiber fracture (IFF), while for the highest damage test cases, a secondary damaged facesheet region is modeled which represents failure to both matrix and fiber constituents.

Three separate material property degradation values are required, one for each region. The elements in the core damage region are reduced to 60% of their initial stiffness. From Fig. 3,

it can be seen that at the point an initially undamaged element reaches compressive failure, the stress is reduced to the stress level at which a damaged element would have obtained. Therefore, the stiffness reduction controls this level, in addition to the damaged element stiffness. The damaged facesheet elements have material properties which were calculated from damaged constituent material properties and a "waviness" factor.

The conservative and non-conservative changes to these material property degradation amounts were as follows. An uncertainty of +/-15% was again used for the damaged core element material property degradation. This means that a non-conservative reduction to 75% and a conservative degradation to 45% of the initial, pristine properties were studied. The values used for matrix and fiber degradation were recommendations from Firehole Composites for use with their software, Helius:MCT. However, in general, these values are based on understanding of experimental results specific to the materials being studied. This is especially true for the matrix degradation value. Fiber degradation is generally less important, as long as it is sufficiently large.

Since a large amount of uncertainty is associated with these values, the values used to study model sensitivity were set as follows. For matrix property degradation, a conservative value of half the damaged stiffness (5%), and a non-conservative value of twice the damaged stiffness (20%) was chosen. (90% degradation for matrix constituent material properties means that these properties are 10% of their initial values.) For the damaged fiber properties, which are 1% of the pristine stiffness, the conservative value of 0.5%, and the non-conservative value of 2% was used. It should be noted that in addition to the degradation of model regions which are modeled as damaged, these stiffness reductions are also used by the Helius:MCT software during the CAI analysis for progressive damage. The sensitivity study takes this into account by adjusting these values as well.

The results of the third and final portion of the sensitivity studies are shown in Table 11. The sensitivity is again shown as a percent change in the CAI failure load. First, the core stiffness reduction value is shown to influence the coupons which fail by indentation propagation more than those which fail by crack propagation, as expected. In fact, for the lightly damaged 6PCF-07 test case, the change in core stiffness reduction has almost no effect. For the more highly damaged case, 6PCF-14, there is another interesting effect. There is increased out-of-plane deformation present

in this test case due to the dent's geometry. Despite the high density core, the large dent depth causes increased though the thickness load transfer from front facesheet to core, causing higher deformation. Fiber stiffness reduction has a very small effect on the overall model result for most test cases, although it is slightly increased for the 6PCF-14 test case. It is recommended that a conservative estimate of stiffness degradation normally be used if there is some question of the nominal value. If fact, in a newer version of the Helius:MCT software package, not used in this research, Firehole Composites reduced the recommended residual stiffness of the fiber constituent from 1% to 0.0001%.

Table 11 Sensitivity study results for element stiffness degradation inputs.

Panel	Input	Percent
3PCF-02	Core stiffness reduction	5.42
	Fiber stiffness reduction	0.00
	Matrix stiffness reduction	2.47
3PCF-16	Core stiffness reduction	5.77
	Fiber stiffness reduction	1.37
	Matrix stiffness reduction	0.89
6PCF-07	Core stiffness reduction	0.04
	Fiber stiffness reduction	0.24
	Matrix stiffness reduction	7.15
6PCF-14	Core stiffness reduction	2.71
	Fiber stiffness reduction	3.92
	Matrix stiffness reduction	2.73

Finally, the change in matrix stiffness degradation has a varied effect on the resulting CAI failure load. In the literature, this value is discussed in regards to the type of progressive failure, the type of matrix cracks present, and their orientation [19] [20]. From observations made during the present research, a specific recommendation would be to implement a gradual degradation approach to matrix failure, as opposed to the single stiffness degradation which is done in the Helius:MCT software for woven composites. This observation is made with regards to the progressive failure analysis, rather then the initial stiffness reduction that is given to the impact damaged regions of the facesheet. In the present research, matrix failure in analysis results is similar to experimental test results. It does not display the large amounts of matrix failure which can be characteristic of a continuum damage model, due to the large stress concentrations considered in CAI analysis.

D. Final Notes on the FEM's Sensitivities

A study of sensitivity to the inputs associated with the new CAI analysis model has been completed. The results are very positive from this study, since most of the changes in failure load observed were very small, given the large changes in the nominal input values which were considered. For some results which did show large changes in CAI failure load for a given input, it was stated that model confidence for these inputs was still high if the uncertainty associated with the actual measurement is very low. The following conclusions can be made which separate model maturity, in the terms of the MATLAB program inputs used into the three categories: "excellent," "good," and "reduced."

For the model inputs for the residual dent depth, the dent diameter, the damaged core region diameter, and the crack length (i.e. length of the fiber fracture region present in the more highly damaged test coupon cases), the model confidence is evaluated to be "excellent." This is based on low sensitivity of the model to these inputs, combined with very high precision with which these measurements were taken. The model confidence in the input which defines the diameter of the facesheet IFF region is only slightly less and is the sole input with confidence defined as "good." The reason for this is slightly reduced precision at which this measurement was taken, but still very low sensitivity of the model to this input. Finally, the confidence associated with the remaining model inputs can be defined as "reduced."

The "reduced" confidence inputs are considered the most reasonable source of any error that may be found in the analysis results when they are compared to the experiments. While all of the inputs are significant to the analysis results, these inputs are in need of the most future attention if the accuracy in the prediction of CAI failure is to be improved. The confidence in the following inputs is considered to be "reduced": the depth of the damaged core region, and the stiffness reduction associated with "damaged" elements in the core, the facesheet IFF region, and the facesheet fiber fracture region. The uncertainty in the core damage depth could be easily improved by refining the model's mesh. However, it was shown that the depth of the core damage has limited impact on the analysis results, as long as some damage is present. The stiffness reduction inputs are the areas of highest uncertainty. The core reduction input should be found in future research through a simple

flatwise core crush test. The matrix and fiber degradation values come from cutting edge areas of composite damage research. With future research, the confidence in these values will increase.

Acknowledgments

This research was completed with the laboratory and financial resources of NASA Langley Research Center (LaRC), in Hampton, VA, through a partnership between NASA LaRC, the National Institute of Aerospace (NIA), and Virginia Tech.

References

[1] McQuigg, T., Kapania, R., Scotti, S., and Walker, S., "Compression After Impact on Honeycomb Core Sandwich Panels with Thin Facesheets, Part 1: Experiments," planned submission to the *53rd AIAA/ASME/ASCE/AHS/ASC Structures, Structural Dynamics and Materials Conference*, Honolulu, Hawaii, 2011.

[2] McQuigg, T., "Compression After Impact Experiments and Analyis on Honeycomb Core Sandwich Panels with Thin Facesheets," Ph.D. Dissertation, Virginia Polytechnic Institute and State University, Blacksburg, VA, May 27, 2011.

[3] Minguet, P., "A Model for Predicting the Behavior of Impact-Damaged Minimum Gage Sandwich Panels Under Compression," *32nd AIAA/ASME/ASCE/AHS/ASC Structures, Structural Dynamics and Materials Conference*, 1991.

[4] Tsang, P., "Impact Resistance and Damage Tolerance of Composite Sandwich Panels," Ph.D. Dissertation, Massachusetts Intitute of Technology, Cambridge, MA, 1994.

[5] Xie, Z., and Vizzini, A., "A Modified Analytical Model for Damage Propagation of a Low-Velocity Impacted Sandwich Panel," *17th ASC Technical Conference on Composite Materials*, West Lafayette, IN, October 2002.

[6] Xie, Z., and Vizzini, A., "Damage Propagation in a Composite Sandwich Panel Subjected to Increasing Uniaxial Compression After Low-Velocity Impact," *Journal of Sandwich Structures and Materials*, Vol. 7, 2005, pp. 269 - 288.

[7] Ratcliffe, J., and Jackson, W., "A Finite Element Analysis for Predicting the Residual Compressive Strength of Impact-Damaged Sandwich Panels," *NASA Technical Report*, NASA/TM-2008-215341, NASA Langley Research Center, Hampton, VA, 2008.

[8] Hwang, Y., and Lacy, T., "Numerical Estimates of the Compressive Strength of Impact-Damaged Sandwich Composites," *Journal of Composite Materials*, Vol. 41, No. 3, 2007, pp. 367 - 388.

[9] Shyprykevich, P., Tomblin, J., Llcewicz, L., Vizzini, A., Lacy, T., and Hwang, Y., "Guidelines for Analysis, Testing, and Nondestructive Inspection of Impact-Damaged Composite Sandwich Structures," *FAA Technical Report*, DOT/FAA/AR-02/121, U.S. Department of Transportation Federal Aviation Administration, Office of Aviation Research, Washington, DC, March 2003.

[10] Xie, Z., and Vizzini, A., "On Residual Compressive Strength Prediction of Composite Sandwich Panels After Low-Velocity Impact Damage," *Sandwich Structures*, Vol. 7, 2005, pp. 363 - 372.

[11] Xie, Z., and Vizzini, A., "The Presence of a Delamination in Damage Growth of an Impacted Sandwich Panel," *16th ASC Technical Conference on Composite Materials*, Blacksburg, VA, September 2001.

[12] Czabaj, M., Zehnder, A., Davidson, B., Singh, A., and Eisenberg, D., "Compression After Impact of Sandwich Composite Structures: Experiments and Modeling," *51st AIAA/ASME/ASCE/AHS/ASC Structures, Structural Dynamics, and Materials Conference*, 2010.

[13] Gibson, L., and Ashby, M., *Cellular Solids: Structure and Properties*, Cambridge University Press, 2nd Ed., 1997.

[14] Aktay, L., Johnson, A., and Kröplin, B.-H., "Numerical Modeling of Honeycomb Core Crush Behavior," *Engineering Fracture Mechanics*, Vol. 75, 2008, pp. 2616 - 2630.

[15] Gornet, L., Marguet, S., and Marckmann, G., "Modeling of Nomex Honeycomb Cores, Linear and Nonlinear Behaviors," *Mechanics of Advanced Materials and Structures*, Vol. 14, 2007, pp. 589 - 601.

[16] Heimbs, S., "Virtual Testing of Sandwich Core Structures Using Dynamic Finite Element Simulations," *Computational Materials Science*, Vol. 45, 2009, pp. 205 - 216.

[17] Kaman, M., Solmaz, M., and Turan, K., "Experimental and Numerical Analysis of Critical Buckling Load of Honeycomb Sandwich Panels," *Journal of Composite Materials*, 2010, pp. 1 - 13.

[18] Dávila, C., Rose, C., and Iarve, E., "Modeling Fracture and Complex Crack Networks in Laminated Composites," *Mathematical Methods and Models in Composites, Computational and Experimental Methods in Structures, V*, Mantič Ed., Imperial College Press, London, UK, accepted for publication, 2011.

[19] Puck, A., and Schürmann, H., "Failure Analysis of FRP Laminates by Means of Physically Based Phenomenological Models," *Composites Science and Technology*, Vol. 58, 1998, pp. 1045 - 1067.

[20] Puck, A., and Schürmann, H., "Failure Analysis of FRP Laminates by Means of Physically Based Phenomenological Models," *Composites Science and Technology*, Vol. 62, 2002, pp. 1633 - 1662.

[21] Garnich, M. and Hansen, A., "A Multicontinuum Theory for Thermal-Elastic Finite Element Analysis of Composite Materials," *Journal of Composite Materials*, Vol. 31, No. 1, 1997, pp. 71 - 86.

[22] Mayes, J. and Hansen, A., "Composite Laminate Failure Analysis Using Multicontinuum Theory," *Composites Science and Technology*, Vol. 64, 2004, pp. 379 - 394.

[23] Helius:MCT Version 3.1, Custom Version Produced for NASA Langley Research Center, Firehole Composites, 2010.

[24] Hasin, Z., "Failure Criteria for Unidirectional Fiber Composites," *Journal of Applied Mechanics*, Vol. 47, 1980, pp. 329 - 334.

[25] "Helius Theory Manual," Firehole Composites, 2009.

[26] Whitcomb, J., and Tang, X., "Effective Moduli of Woven Composites," *Journal of Composite Materials*, Vol. 35, No. 23, 2001, pp. 2127 - 2144.

[27] Searles, K., Odegard, G., and Kumosa, M., "Micro- and Mesomechanics of 8-harness Satin Woven Fabric Composites: I - Evaluation of Elastic Behavior," *Composites: Part A*, Vol. 32, 2001, pp. 1627 - 1655.

[28] Gao, X.-L., Li, K., and Mall, S., "A Mechanics-of-Materials Model for Predicting Young's Modulus of Damaged Woven Fabric Composites Involving Three Damage Modes," *International Journal of Solids and Structures*, Vol. 40, 2003, pp. 981 - 999.

[29] Angioni, S., Meo, M., and Foreman, A., "A Comparison of Homogenization Methods for 2-D Woven Composites," *Composites: Part B*, Vol. 42, 2011, pp. 181 - 189.

[30] Hyer, M., *Stress Analysis of Fiber-Reinforced Composite Materials*, WCB/McGraw-Hill, 1998, out-of-print.

[31] "ACG MTM45-1 6781 S-2 glass 35% RC," *Qualification Material Statistical Analysis Report*, CAM-RP-2009-001, National Center for Advanced Materials Performance, NASA, National Institute for Aviation Research, Wichita State University, KS, February 2010.

[32] "HexWeb Honeycomb Attributes and Properties," HexCel Composites, Inc., 1999, URL: `http://www.hexcel.com/Resources/DataSheets/Brochure-Data-Sheets/Honeycomb_Attributes_and_Properties.pdf` [cited June 21, 2011].